Transport in Porous Media manuscript No.
(will be inserted by the editor)

Landfill gas flow: collection by horizontal wells

Yana Nec · **Greg Huculak**

Received: / Accepted:

Abstract Collection of landfill gas by horizontal perforated wells is studied. The problem combines flow through porous media in the landfill and unobstructed pipe flow in the well. Respective analytical solutions to flow equations are used in an iterative numerical procedure to solve the coupled system. Realistic landfill input parameters confirm the feasibility of estimates obtained with the model. The study identifies flow control parameters and furnishes tools to evaluate surface flux and radius of influence for this type of well.

Keywords landfill gas flow · horizontal well · multiple layer porous media · surface flux · radius of influence

PACS 47.56.+r · 47.85.M- · 88.05.Np · 88.20.dv

Mathematics Subject Classification (2010) 76S05

1 Background

Landfill gas is generated by an anaerobic degradation of compacted waste and comprises a mixture of CH_4, CO_2, O_2 and N_2. Although regimes of flow through a solid matrix can be broadly catalogued for instance by Reynolds number (Fand et al., 1987), additional complications might arise, consult e.g. Lage et al. (1997) and references therein. For landfill gas the thermodynamic and flow conditions involve no excessive pressure or temperature, and low Reynolds and Mach numbers. Hence it is possible to use the ideal gas equation of state

$$p = \rho RT, \quad R = R_o \Big/ \sum_i x_i M_i, \tag{1}$$

where p, ρ and T denote static pressure, fluid density and temperature respectively. R_o is the universal gas constant, and x_i, M_i stand for component molar fractions and weights.

Historically landfill construction developed with scarce research in the field of flow theory. The main concerns were centred around gas generation by various types of waste, efficient extraction, safety of operation and environmental aspects. Comprehensive literature exists on leachate and contaminants, however surprisingly few studies address the flow of landfill gas itself. A numerical solution was obtained for a one-dimensional flow to a passive vertical vent (Chen et al., 2003), and a well with dynamic extraction using two-dimensional geometry (Yu et al., 2009), referencing a small number of analogous studies. Two recent contributions analysed a configuration of multiple wells, vertical and horizontal (Feng et al., 2015, 2017). All foregoing works use an extensive number of input parameters. In practice the consequence is twofold: one, it is

Y. Nec
Department of Mathematics and Statistics, Thompson Rivers University, Kamloops, British Columbia, Canada
Tel.: 1250-852-7831
E-mail: cranberryana@gmail.com

G. Huculak
GNH Consulting Ltd., Delta, British Columbia, Canada

difficult to predict what impact a change in one parameter would have on the solution; and two, distinct sets of parameters might result in very close solutions. In conjunction with the high uncertainty of the physical properties of the waste matrix, such an underdetermined system can easily fit field data, nevertheless failing to provide a design engineer or operator with practical means of understanding and controlling gas collection. In the current contribution the flow toward and within a horizontal well is solved with a minimal number of parameters, explicating several control related phenomena experienced in the field: (A) poor or no response of the mass collected to variation in the induced sub-atmospheric outlet pressure; (B) failure to collect the expected mass despite application of sufficient suction strength even for the type of waste generating large quantities of gas; (C) air infiltration and overextraction.

Horizontal wells collect gas through apertures along their entire length, thereby being conceptually distinct from the traditional vertical wells. A landfill utilising horizontal well collection is constructed as follows. In the centre, at a selected depth, a perforated pipe is placed, surrounded by gravel. Gas generating waste extends radially from this core that acts as a filter, preventing clogging of collection apertures. A low permeability cover layer or a sealing membrane might be added. The layers around the well form the flow domain with each layer a sub-domain or lamina. Sub-atmospheric pressure is imposed at the pipe outlet, the other end blocked. Figure 1 shows schematics and notation detail.

Permeability as a characteristic of a porous medium has attracted substantial interest, from experimental estimates and to the theory of interaction between the fluid and medium geometry. A thorough classification of concepts underpinning fluid passage through a stationary structure is given in the introductory part of Panda and Lake (1994), and a relation is derived linking the permeability k to the attributes of porosity $0 < \phi < 1$ and tortuosity $\tau > 0$, known as the Kozeny-Carman equation:

$$k = \frac{\phi^3 r_{\textcircled{\scriptsize C}}^2}{18\tau(1-\phi)^2}, \tag{2a}$$

where $r_{\textcircled{\scriptsize C}}$ denotes the radius of an equivalent spherical particle, related to the matrix hydraulic radius by

$$r_{\mathrm{H}} = \phi r_{\textcircled{\scriptsize C}} \Big/ \Big(3(1-\phi)\Big). \tag{2b}$$

The main part of that work connects the permeability to the probability density function of the particle size in a non-uniform porous matrix. A conceptually distinct study employs the theory of fractals to arrive at a generalised relation that includes (2a) as well as numerous variants as special cases (Henderson et al., 2010). References within give an overview of the numerous modifications the original notion of Carman (Carman, 1937) has seen over time.

Flow through porous media is an actively studied subject. What renders few contributions in this field applicable to landfill gas flow is the unpredictability of the matrix properties. Thus only the most generic studies can help make adequate decisions on the choice of governing equations or conditions. Allan et al. (2008) analysed a three layer medium, with only the middle layer being of finite dimensions. Albeit the equations were more complicated, Forchheimer and Brinkman equations – Darcy's law with a non-linear term and a correction for media grains that are porous themselves respectively, the laminar flow regime, continuity conditions and main non-dimensional parameters, Reynolds and Darcy numbers, are pertinent. Modelling a fully realistic landfill gas flow is encumbered both by medium anisotropy and a fluid that combines gas and liquid in the form of leachate. Generic studies on multi-scale permeability and multi-phase flow might furnish a good starting point for future modelling, cf. Nakshatrala et al. (2018) and Bahloul et al. (2005), as well as references therein. However before such advanced modelling is attempted, it is imperative to understand the basic flow of gas through a domain comprising all relevant landfill layers. In light of the above in equation (2a) all parameters are regarded as effective quantities to be evaluated through experience or reliable sources of industry data within each sub-domain.

2 Governing equations

The continuity equation balances a source C and the mass of fluid flowing through a control volume, whose storage ability is limited by $0 < \phi < 1$ (Fulks et al., 1971):

$$\frac{\partial}{\partial t}(\phi\rho) + \nabla\cdot(\rho\mathbf{u}) = C, \tag{3a}$$

$$\nabla\cdot(\rho\mathbf{u}) = \frac{1}{r}\frac{\partial}{\partial r}(r\rho u) + \frac{1}{r}\frac{\partial}{\partial\theta}(\rho v) + \frac{\partial}{\partial\ell}(\rho w), \tag{3b}$$

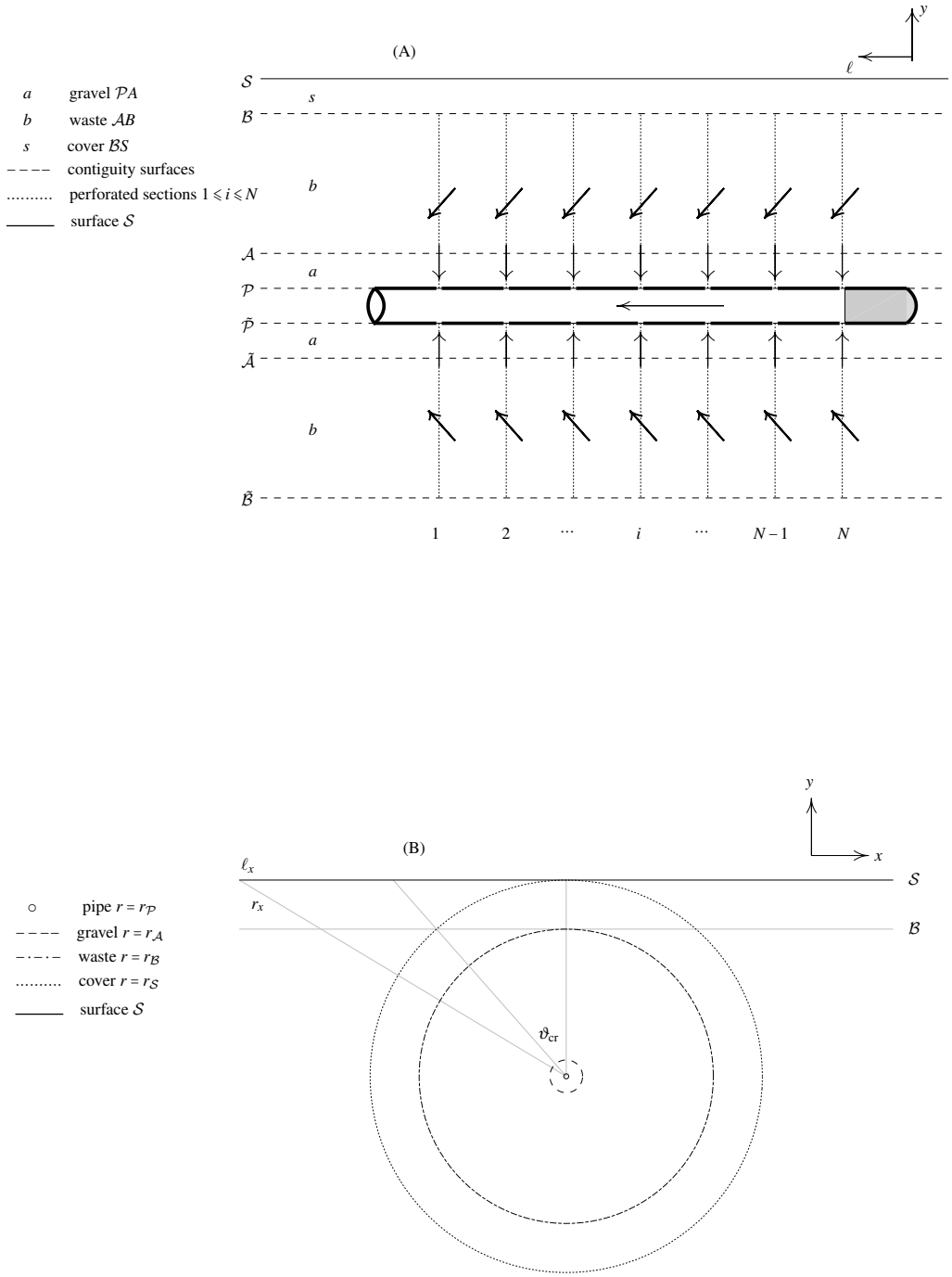

Fig. 1 Flow geometry. Side view (A): perforated pipe imbedded within media of distinct permeability. The perforated cross-sections are indexed from the well outlet. Arrows mark general direction of flow. Cross-section (B): ℓ_x denotes horizontal distance for surface flux computation, ϑ_{cr} marks the angle, where tangent $\mathcal{B}$ to circle of radius $r_{\mathcal{B}}$ intersects circle of radius $r_{\mathcal{S}}$. Dimensions not to scale.

where u, v and w are the radial, azimuthal and longitudinal fluid velocities respectively, $\mathbf{u} = (u, v, w)^{\mathrm{T}}$ being the velocity vector in polar coordinates $\mathbf{x} = (r, \theta, \ell)$ with the angle θ measured positive counter-clockwise from the horizontal through the pipe centre. C is the volumetric generation rate.

For a flow in a porous medium the conservation of momentum is given by Darcy's law, in the absence of gravity reading (Whitaker, 1986):

$$\mathbf{u} = -\frac{\bar{\bar{\mathbf{K}}}}{\mu} \nabla p. \tag{4a}$$

Generally the entries k_{ij} in the tensor $\bar{\bar{\mathbf{K}}}$ are permeability values for flow in direction i under pressure gradient imposed in direction j. The viscosity μ of a mix of ideal gases is computed as in Davidson (1993). In polar coordinates

$$\nabla p = \left(\frac{\partial p}{\partial r}, \ \frac{1}{r}\frac{\partial p}{\partial \theta}, \ \frac{\partial p}{\partial \ell} \right)^{\mathrm{T}}. \tag{4b}$$

For an isotropic medium $\bar{\bar{\mathbf{K}}}$ reduces to a scalar permeability k, distinct for each sub-domain and regarded as an effective value in the presence of anisotropy. Combining (3), (4) and (1) for a steady axisymmetric flow gives

$$\frac{1}{r}\frac{\partial}{\partial r}\left(r \frac{\partial}{\partial r} p^2 \right) + \frac{\partial^2}{\partial \ell^2} p^2 = -\frac{2\mu}{k} RTC. \tag{5}$$

All fluid and medium properties, including the generation rate C, are taken constant to allow for a deterministic solution to be tested with feasible ranges of parameters that otherwise can only be modelled probabilistically. The assumption of axial symmetry is essential to obtain an analytical solution.

The flow through the landfill's porous layers is coupled to a weakly compressible flow in the well. Since at each perforated section gas is coming in, some flow parameters are segment specific. Without loss of generality assign the index $i = 0$ to the outlet section and let segment i lie between sections $i-1$ and i for any $i = \{1, \ldots, N\}$ as in figure 1. Designating the mass flow rate in segment i by $\dot{m}_i$ and the friction coefficient by f_i, the well pressure obeys the following equation (Nec and Huculak, 2017):

$$\frac{dp}{d\ell} = \frac{f_i p}{4 r_{\mathcal{P}}} \Bigg/ \left(1 - \frac{\pi^2 r_{\mathcal{P}}^4 p^2}{\dot{m}_i^2 RT} \right). \tag{6a}$$

Here $r_{\mathcal{P}}$ is the pipe radius, and the Darcy friction coefficient f_i is obtained from the Colebrook equation (Colebrook, 1939)

$$\frac{1}{\sqrt{f_i}} = -2\log_{10}\left(\frac{\varepsilon}{3.7} + \frac{2.51}{\mathrm{Re}_i \sqrt{f_i}} \right), \tag{6b}$$

where Re_i is the Reynolds number in segment i and ε stands for the non-dimensional roughness of the pipe inner surface, both based on the pipe diameter. Integration of (6a) over segment i delimited by the points ℓ_{i-1} and ℓ_i gives

$$\frac{4 r_{\mathcal{P}}}{f_i} \ln \frac{p_{i-1}}{p_i} - \frac{2\pi^2 r_{\mathcal{P}}^5}{f_i \dot{m}_i^2 RT} \left(p_{i-1}^2 - p_i^2 \right) = \ell_i - \ell_{i-1}. \tag{6c}$$

Additional technical detail may be found in Nec and Huculak (2017).

2.1 Combined system

The partial differential equation (5) is coupled with the system of n non-linear transcendental equations (6c) through both the influx $\Delta \dot{m}_i$ and pressure p_i at the perforated sections. The open domain for the landfill flow in the (r, ℓ) plane is $\Omega = (r_{\mathcal{P}}, r_{\mathcal{X}}) \times (0, L)$, where L is the total length of the well. The outer radius $r_{\mathcal{X}}$ equals either $r_{\mathcal{B}}$ or $r_{\mathcal{S}}$, depending on whether the cover is impervious, constituting a boundary, or permeable, forming a third porous lamina. Equation (5) must be solved in Ω, comprising hollow contiguous cylinders with concomitant permeabilities k. The generation rate C vanishes in the gravel and cover laminae $\mathcal{P}A$ and $\mathcal{B}S$, $\left\{ (r, \ell) \,\middle|\, r_{\mathcal{P}} \leqslant r \leqslant r_{\mathcal{A}}, \quad r_{\mathcal{B}} \leqslant r \leqslant r_{\mathcal{S}} \right\}$. The boundary conditions on the closure $\partial\Omega$ are set hereinafter for the different cases. On all inner surfaces of contiguity between media of distinct properties continuity of pressure and velocity must hold.

2.1.1 Quasi-one-dimensional formulation

One possibility is to construct a quasi-one-dimensional solution based on a purely radial flow within each plane corresponding to a perforated cross-section. The validity of this approach requires a twofold substantiation. The first point is to show that a planar description is a good approximation, representing the apertures as axisymmetric slits of equivalent area and sufficiently narrow width. Taking n_h holes of radius r_h sufficiently small relative to $r_{\mathcal{P}}$ for the hole to be assumed circular, the width of the required slit δ satisfies

$$\frac{\delta}{r_{\mathcal{P}}} = \frac{n_h}{2}\left(\frac{r_h}{r_{\mathcal{P}}}\right)^2 \ll 1, \tag{7}$$

so indeed the representation is planar. The second point is to show that changes in the longitudinal direction within the landfill are small. The mapping $r \longmapsto r_{\mathcal{P}} r'$, $\ell \longmapsto L\ell'$, r' and ℓ' being non-dimensional radius and length, casts equation (5) into the form

$$\frac{1}{r'}\frac{\partial}{\partial r'}\left(r'\frac{\partial}{\partial r'}p^2\right) + \left(\frac{r_{\mathcal{P}}}{L}\right)^2 \frac{\partial^2}{\partial \ell'^2}p^2 = -\frac{2\mu}{k}RTCr_{\mathcal{P}}^2. \tag{8}$$

The ratio $r_{\mathcal{P}}\big/L$ is extremely small. Even if the representative radial dimension was chosen as the depth $r_{\mathcal{X}}$ rather than $r_{\mathcal{P}}$, this quantity would still be very small. Therefore the longitudinal term in equation (5) is much smaller than the radial term, longitudinal changes are small, and a quasi-one-dimensional representation is reasonable. As regards the numerical implementation, estimates (7) and (8) allow to reduce the landfill to a set of thin generating slices of width $\delta/r_{\mathcal{P}}$ located at longitudinal coordinates ℓ_i, $i = \{1,\dots,N\}$. The slice aligned with the perforated section ℓ_i is responsible for collection of gas generated in the segment $\ell_{i-1} < \ell < \ell_i$.

With longitudinal variation neglected, (5) takes the form

$$\frac{1}{r}\frac{d}{dr}\left(r\frac{d}{dr}p^2\right) = -\frac{2\mu}{k(r)}RTC(r), \tag{9a}$$

$$k(r) = \begin{cases} k_a & r_{\mathcal{P}} < r < r_{\mathcal{A}} \\ k_b & r_{\mathcal{A}} < r < r_{\mathcal{B}} \\ k_s & r_{\mathcal{B}} < r < r_{\mathcal{S}} \end{cases}, \quad C(r) = \begin{cases} 0 & r_{\mathcal{P}} < r < r_{\mathcal{A}} \\ C_b & r_{\mathcal{A}} < r < r_{\mathcal{B}} \\ 0 & r_{\mathcal{B}} < r < r_{\mathcal{S}} \end{cases}. \tag{9b}$$

Here k_a, k_b and k_s are permeabilities of laminae $\mathcal{P}A$, $\mathcal{A}B$ and $\mathcal{B}S$ respectively, and C_b denotes the effective generation rate within $\mathcal{A}B$. At the contiguity surface $r = r_{\mathcal{A}}$ and if applicable also at $r = r_{\mathcal{B}}$ continuity of pressure and velocity must hold. Denoting the relevant radii by $r_{\mathcal{I}}$ and permeabilities of respective laminae below and above by k_- and k_+,

$$p\left(r_{\mathcal{I}}^-\right) = p\left(r_{\mathcal{I}}^+\right), \qquad k_- p'\left(r_{\mathcal{I}}^-\right) = k_+ p'\left(r_{\mathcal{I}}^+\right). \tag{9c}$$

Equation (9a) must be solved for each plane aligned with a perforated section with the following boundary conditions. At the outer boundary $r_{\mathcal{X}}$, $r_{\mathcal{X}} \in \{r_{\mathcal{B}}, r_{\mathcal{S}}\}$,

$$p(r_{\mathcal{X}}) = p_{\mathcal{X}} \qquad \text{or} \qquad u(r_{\mathcal{X}}) = 0. \tag{9d}$$

In the case $p(r_{\mathcal{X}}) = p_{\mathcal{X}}$ the prescribed value $p_{\mathcal{X}}$ is either the barometric pressure or a slightly sub-atmospheric value expected under the cover. The case $u(r_{\mathcal{X}}) = 0$ represents a situation where an impervious membrane is installed. At the well boundary

$$p(r_{\mathcal{P}}) = p_i, \quad i = \{0,\dots,N\}, \tag{9e}$$

where p_0 is a given outlet pressure. The values p_i for $1 \leqslant i \leqslant N$ are related through (6c) and can only be computed consecutively from the well outlet. Conservation of mass must hold at each perforated section. Denoting by $\Delta\dot{m}_i$ the mass incoming at section i,

$$\dot{m}_{i-1} = \dot{m}_i + \Delta\dot{m}_{i-1}, \quad i = \{2,\dots,N\}. \tag{9f}$$

Thus an initial guess for the mass flow m_1 must be made and system (9) solved iteratively, so at the last flowing segment

$$\dot{m}_N = \Delta\dot{m}_N. \tag{9g}$$

System (9) forms the closed mathematical problem for the quasi-one-dimensional case.

2.1.2 Two-dimensional formulation

Retaining the longitudinal variation, equation

$$\frac{1}{r}\frac{\partial}{\partial r}\left(r\frac{\partial}{\partial r}p^2\right)+\frac{\partial^2}{\partial \ell^2}p^2=-\frac{2\mu}{k(r)}RTC(r),\quad (r,\ell)\in\Omega \tag{10a}$$

must be solved with $k(r)$ and $C(r)$ as in (9b). Conditions (9c) and (9d) remain, formally written for all $\ell\in[0,L]$ as

$$p\big(r_{\mathcal{I}}^-,\ell\big)=p\big(r_{\mathcal{I}}^+,\ell\big),\quad k_-\left.\frac{\partial p}{\partial r}\right|_{(r_{\mathcal{I}}^-,\ell)}=k_+\left.\frac{\partial p}{\partial r}\right|_{(r_{\mathcal{I}}^+,\ell)}, \tag{10b}$$

$$p(r_{\mathcal{X}},\ell)=p_{\mathcal{X}}\quad\text{or}\quad u(r_{\mathcal{X}},\ell)=0. \tag{10c}$$

Condition (9e) becomes

$$p(r_{\mathcal{P}},\ell)=p_{\text{in}}(\ell), \tag{10d}$$

where $p_{\text{in}}(\ell)$ is the pressure within the well, varying continuously in accord with (6a). Thus conceptually this formulation does not require a reduction of the landfill domain into thin slices. Notwithstanding, due to the inevitable discretisation of the function $p_{\text{in}}(\ell)$ in the numerical implementation, the two-dimensional and quasi-one-dimensional formulations are equivalent in this respect. Additional conditions for this case are

$$w(r,L)=0,\qquad r\in[r_{\mathcal{P}},r_{\mathcal{X}}], \tag{10e}$$

i.e. no horizontal flux across the plane $\ell=L$, corresponding to the end of the well, and finally at the outlet

$$p(r,0)=p_{\text{out}}(r),\qquad r\in[r_{\mathcal{P}},r_{\mathcal{X}}], \tag{10f}$$

where $p_{\text{out}}(r)$ must be consistent with the other boundary conditions, namely satisfy $p_{\text{out}}(r_{\mathcal{P}})=p_{\text{in}}(0)=p_0$ and either $p_{\text{out}}(r_{\mathcal{X}})=p_{\mathcal{X}}$ or $p'_{\text{out}}(r_{\mathcal{X}})=0$ by (10c). Relations (9f) and (9g) complete the system for the two-dimensional case.

System (10) must be solved iteratively, however in contrast to (9) the initial guess must encompass the entire well length, e.g. mass flow rates $\dot{m}_i$ within all segments to yield $p_{\text{in}}(\ell)$ by (6a). With this as a tentative boundary condition, (10a) is solved for $p(r,\ell)$, whose radial derivative is then evaluated at $(r_{\mathcal{P}},\ell_i)$, giving influx $\Delta\dot{m}_i$ and thence $\dot{m}_i$ by (9f) and (9g), serving to adjust the initial guess until convergence.

In summary, (9) and (10) are non-linear differential-algebraic systems, qualitatively modelling a multi-layer landfill coupled to a horizontal well. Conservation of mass and continuity of pressure across the perforated pipe surface underpin the coupling mechanism between the two flow fields in the implementation of the iterative scheme. For consistence with the assumption of axial symmetry the apertures are regarded as thin slits of equivalent area. Head losses due to ingress into the pipe are not modelled, but might be represented through the effective permeability of the gravel layer.

Hereinafter systems (9) and (10) are solved subject to boundary conditions reflecting possible operational configurations with the aim to formulate flow control strategies. Fitting field data, accuracy of prediction and full parameter space investigation are outside of the scope of this study.

3 Analytical solution for landfill flow

The iterative solution of the landfill-well coupled systems (9) and (10) requires the pressure profiles within a single landfill cross-section by equations (9a) and (10a) respectively. These are obtained analytically as follows.

3.1 Radial flow

The mathematical problem (9a) – (9d) comprises four cases: the outermost domain radius is $r_{\mathcal{X}} \in \{r_{\mathcal{B}}, r_{\mathcal{S}}\}$, where either pressure value or zero velocity is imposed. Within any one lamina, i.e. with constant k and C, (9a) is solved as

$$p^2 = -\frac{\mu}{2k} RTCr^2 + a^{(0)} \ln r + b^{(0)}, \tag{11}$$

where $a^{(0)}$ and $b^{(0)}$ are integration constants, determined from (9b) – (9d) by a linear system, whose size is twice the number of laminae in Ω, here either four ($r_{\mathcal{X}} = r_{\mathcal{B}}$) or six ($r_{\mathcal{X}} = r_{\mathcal{S}}$). The solutions are instructive from the aspects detailed below, whilst the expressions for $a^{(0)}$ and $b^{(0)}$ are given in appendix B due to cumbersomeness.

The boundary condition $p(r_{\mathcal{B}}) = p_{\mathcal{B}}$ is pertinent to two situations. One, the landfill is uncovered and $p_{\mathcal{B}}$ equals the barometric pressure. Two, a permeable cover is in place, but the desired solution domain excludes it. Then $p_{\mathcal{B}}$ is chosen slightly sub-atmospheric. At first glance such an arrangement might appear peculiar, however it is not without merit. It allows the operator to test the response to variation in outlet pressure p_0 over a range of medium permeabilities and ensuing head loss across each lamina and along the well. All this is possible even if the generation rate C_b is set to zero, which permits faster convergence of the quasi-one-dimensional iterative solution, as well as spares the need to supply one more input parameter.

If $C_b = 0$, the case $p(r_{\mathcal{B}}) = p_{\mathcal{B}}$ yields a reasonable approximation to the situation of moderate to low generation. The radial pressure profile is then square root logarithmic. If $C_b > 0$, the profile involves a parabola as an additive term to the logarithm, no longer monotonic for a combination of high generation and insufficient outlet suction, with pressure mounting to above atmospheric within the landfill.

Cases $u(r_{\mathcal{B}}) = 0$ and $u(r_{\mathcal{S}}) = 0$ can be unified, since the pressure is uniform within the cover lamina and equals the pressure attained at the point $r = r_{\mathcal{B}}$, where the radial velocity vanishes. Both cases result in a stagnant landfill if $C_b = 0$.

Purely radial flow is the only setting, where mass is conserved across confocal circles. With longitudinal coupling no such conservation holds, axial symmetry notwithstanding.

3.2 Radial-longitudinal flow

System (10) is solved by separation of variables in conjunction with a non-homogeneous term

$$p^2 = -\frac{\mu}{2k} RTCr^2 + P(r)A(\ell), \tag{12}$$

the functions $P(r)$ and $A(\ell)$ to be found from (10a). Condition (10e) implies $A'(L) = 0$, and from (10f) follows that $A(0) = 1$. The generalisation of (11) is then

$$p^2 = -\frac{\mu}{2k} RTCr^2 + a^{(0)} \ln r + b^{(0)} + \sum_{n=1}^{\infty} \cos \tilde{\ell} \left(a^{(n)} I_0(\tilde{r}) + b^{(n)} K_0(\tilde{r}) \right), \tag{13a}$$

wherein I_ν and K_ν are modified Bessel functions of order ν of first and second kinds respectively, and

$$\tilde{\ell} = \lambda_n \ell, \quad \tilde{r} = \lambda_n r, \quad \lambda_n = \pi n \big/ L. \tag{13b}$$

The coefficients $a^{(n)}$ and $b^{(n)}$ are determined by (10b) – (10d) for each lamina with concomitant k and C given by (9b). The solutions to the linear system ensuing require identities satisfied by Bessel functions (Gradshteyn and Ryzhik, 2007) and are given in appendix C for $n \geqslant 1$. For $n = 0$ they are identical to those in the quasi-one-dimensional solution upon mapping $p_i^2 \longmapsto \frac{1}{L} \int_0^L p_{\text{in}}^2(\ell) d\ell$, arising when imposing (10d) instead of the discrete (9e), and thus need not be restated.

The terms preceding the sum in (13a) coincide in form with the one-dimensional solution (11). Since the sequences $a^{(n)}$ and $b^{(n)}$ must diminish in magnitude with sufficient rapidity as $n \longrightarrow \infty$ for the series to be convergent, the foregoing terms are also expected to give the leading order in magnitude. This was ascertained with realistic data (appendix A). Thus the importance of the quasi-one-dimensional solution reaches beyond a mere simplification. Moreover, it constitutes a valuable initial guess for a proper convergence of the iterative solution of the two-dimensional problem.

For the cases $p(r_{\mathcal{X}},\ell) = p_{\mathcal{X}}$ the infinite series manifests a rapid convergence. As few as 15 terms suffice for all practical purposes. For the solutions presented in §4 a verification of convergence was performed with the number of terms doubled, always yielding graphically indistinguishable results. For the cases $u(r_{\mathcal{X}}) = 0$ the series convergence is sensitive to input parameters, albeit each term satisfies the vanishing velocity boundary condition independently. Using this solution is practicable only if C_b is large enough. With the value used throughout in §4 convergence was attained with the same number of terms as for the pressure boundary condition.

4 Numerical solution

The devised iterative scheme combined the analytical solutions in §3 with the non-linear pressure dependence within the well (6c) and the closure equation (9g) to solve the coupled systems (9) and (10). This section illustrates the flow field in the landfill and well interior. A set of parameters common to all examples is listed in appendix A. All quantities are characteristic of medium sized landfills and have been verified to give robust results, to wit moderate deviations in these values effect no qualitative change in the solution. Pressure values shown without a reference point are relative to atmospheric. In the iterative solution of system (9) the convergence tolerance was 10^{-7} for the relative error $(\Delta\dot{m}_N - \dot{m}_N)/\Delta\dot{m}_N$, cf. equation (9g). For system (10) same tolerance was used for the relative error on the second norm of the function $p_{\text{in}}(\ell)$ computed at successive iterations j and $j+1$: $\left\|p_{\text{in}}^{(j+1)}(\ell) - p_{\text{in}}^{(j)}(\ell)\right\| \Big/ \left\|p_{\text{in}}^{(j)}(\ell)\right\|$.

4.1 Effect of boundary conditions

Figure 2 gives a typical solution of the combined flow field for a condition of the type $p(r_{\mathcal{B}}) = p_{\mathcal{B}}$, applicable when a permeable cover was excluded from the formal solution domain. The outlet suction was chosen so as to span the entire physical range of qualitatively distinct solutions: with $p_{\text{out}} = -1.25$kPa landfill gas will accumulate if a cover is in place or escape in the absence thereof, whereas with $p_{\text{out}} = -2.5$kPa overextraction will occur or air will be drawn in. At both extremities the quasi-one-dimensional and two-dimensional solutions are visually indistinguishable. The Reynolds number (equivalent to flow rate) varies virtually linearly along the well, as confirmed by an almost uniform intake of fluid throughout its length. Observe the response to variation in outlet pressure: a suction of a double magnitude resulted in a close to double gas collection. The response of the pressure gradient along the well is non-linear, of course. The pressure profile in the landfill domain shows that most of the head present at each perforation dissipates within the gravel layer. For $r > r_{\mathcal{A}}$ the solution is virtually constant and thus not shown.

Figure 3 depicts the solution for a condition of the type $u(r_{\mathcal{B}}) = 0$, suitable for a sealed cover. The radial variation of pressure in the landfill is more gradual, cf. the gradients over the gravel layer with those in figure 2. The quasi-one-dimensional and two-dimensional solutions are close, but not fully in agreement. Outlet suction has virtually no impact on the head loss and flow rate within the well. Therefore with an impervious cover the amount of gas collected is determined solely by the effective permeability properties. The inability to control the flow rate by induction of a stronger suction at the outlet has baffled field operators, and this phenomenon is predicted here. Nevertheless an adequate suction will be required to maintain a slightly sub-atmospheric pressure throughout in order to prevent landfill gas accumulation or escape around the cover edges, even if the same amount of gas might be collected with a much weaker outlet suction.

In light of the above, the outermost surface boundary condition is related to the controllability of flow rate and collected mass of gas. Albeit the uppermost part of the waste lamina is virtually stagnant for both $p(r_{\mathcal{B}},\ell) = p_{\mathcal{B}}$ and $u(r_{\mathcal{B}},\ell) = 0$, the conceptual distinction remains: when pressure is prescribed, the radial velocity, howsoever small, mathematically does not vanish, whilst with zero velocity imposed, the pressure varies longitudinally and thus cannot be tuned to match barometric. Varying the suction strength permits to control the amount of gas collected in the former case, but proves ineffectual in the latter. The quasi-one-dimensional and two-dimensional solutions give nearly identical results. When a minor difference is visible in flow properties local to the perforated sections, the impact on cumulative quantities is negligible. In all results discussed hereunder solutions to (9) and (10) were indistinguishable with only the former shown.

4.2 Effects of permeability ratio

The nominal set of parameters (appendix A) corresponds to a loosely packed refuse, i.e. the permeability of the waste lamina exceeds that of the gravel. Figure 4 compares that solution, $k_b/k_a \approx 30$, with the case of closely compacted waste,

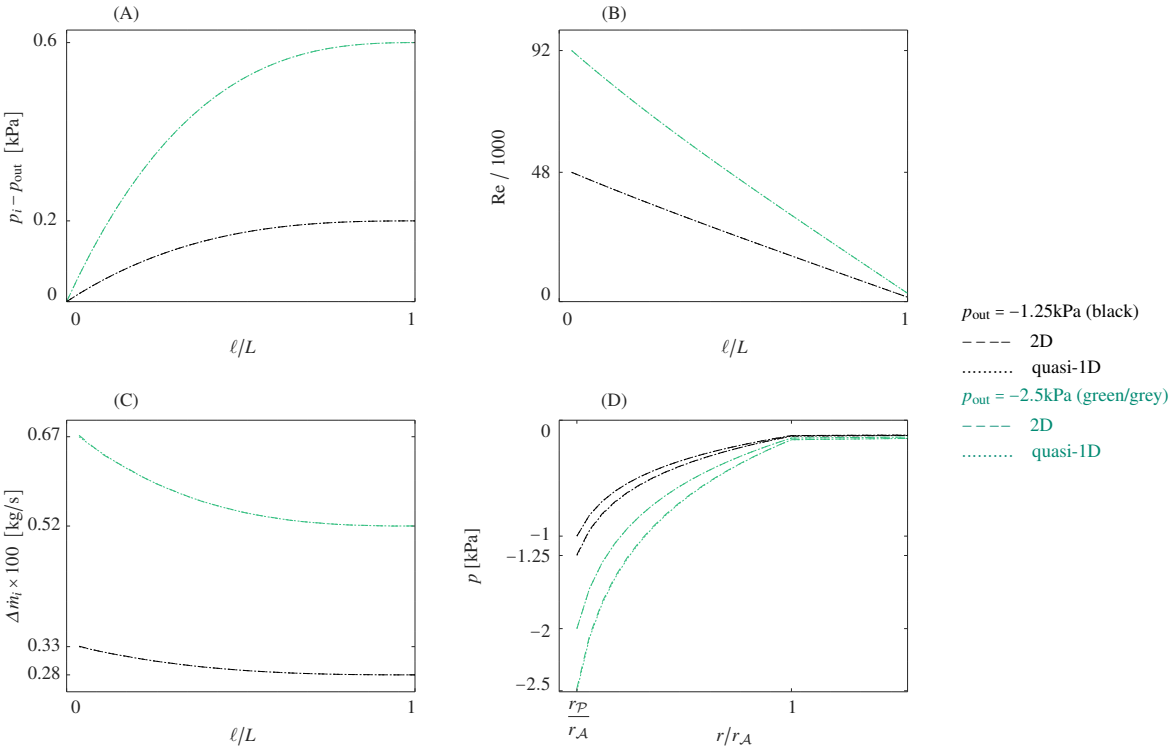

Fig. 2 Quasi-one-dimensional and two-dimensional solutions (systems (9) and (10) respectively): pressure variation in the well (A); respective Reynolds number (B); aperture influx (C); radial pressure profiles in the landfill (D) for outlet and last flowing cross-sections (rightmost, $\ell = 0$, and leftmost, $\ell = L$, curves of identical style respectively). Boundary condition $p(r_{\mathcal{B}}) = -0.125$kPa. All other parameters listed in appendix A.

so that $k_b/k_a \approx 0.3$. It is evident a more compact packing would require the exertion of a stronger outlet suction to extract the same amount of gas. In this unequivocal setting this is an intuitive result. In practice, however, a medium of a smaller permeability often consists of waste such as organic matter, expected to generate more gas, and notwithstanding, the mass collected appears unreasonably low. The salient physical reason is seen in the landfill pressure profile: because the ratio k_b/k_a is small, the head available at the well apertures dissipates more gradually, attaining a super-atmospheric pressure before attenuation towards the prescribed boundary value. This is an indication of gas accumulation that needs to be resolved either by a stronger outlet suction, or as is shown below, by a higher perforation density. Here quasi-one-dimensional and two-dimensional solutions were identical. The solution with $u(r_{\mathcal{B}}) = 0$ is qualitatively similar and not shown.

4.3 Cover lamina

Condition $p(r_{\mathcal{S}}) = p_{\mathcal{S}}$ incorporates a third lamina as part of the formal solution domain. Most often the cover consists of fine particle soil with permeability k_s smaller than that of both inner laminae. Figure 5 confirms that the presence of a cover will require a stronger outlet suction to maintain sub-atmospheric pressure throughout the landfill, since an additional lamina always entails further flow resistance, definitely so if $k_s < k_a, k_b$.

When solving without a cover, the condition is prescribed at the outermost surface of the waste lamina $r = r_{\mathcal{B}}$, where it is desirable that $p(r_{\mathcal{B}})$ be slightly below the barometric pressure p_{bar}. With the cover an integral part of the solution domain, p_{bar} is set at the surface $r = r_{\mathcal{S}}$. If it was possible to guess $p(r_{\mathcal{B}})$ rather than estimate it, the two solutions would coincide for all $r \leqslant r_{\mathcal{B}}$. Moreover, it will be possible to obtain the solution in $r_{\mathcal{B}} < r \leqslant r_{\mathcal{S}}$ by extension as in §5. However in practice landfill covers are at times removed to add more refuse or allow for pipework repair, the landfill in fact operating without a

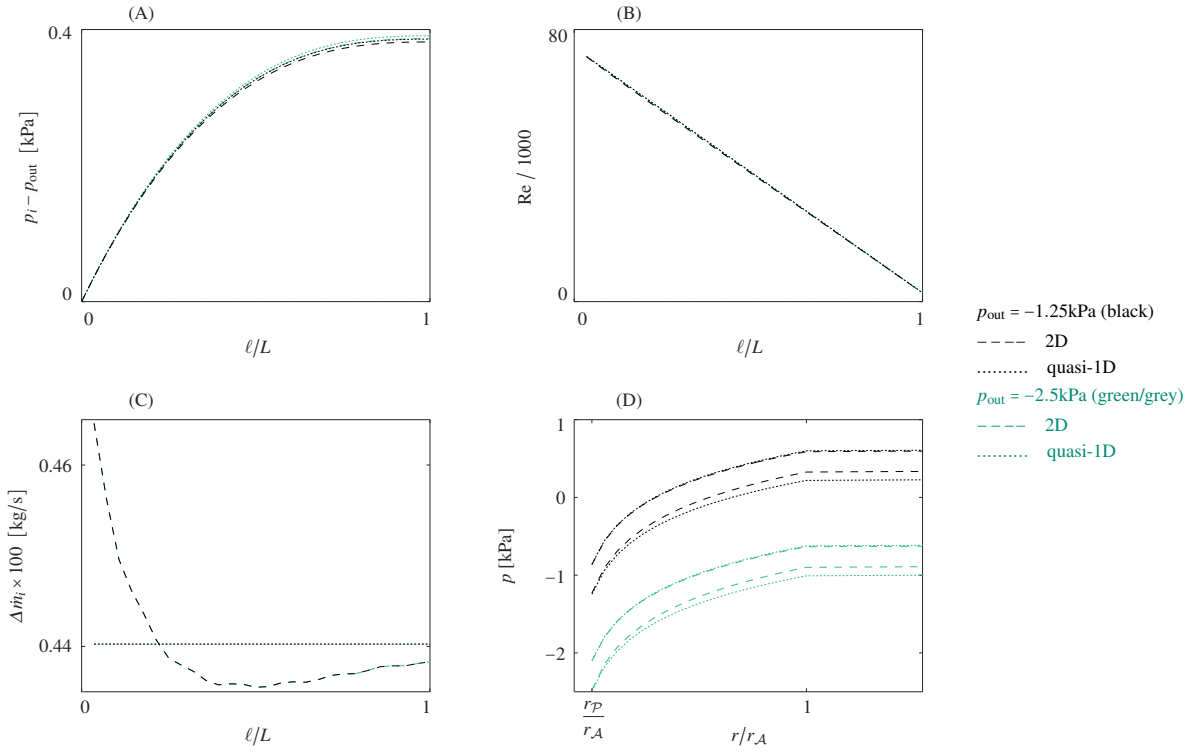

Fig. 3 Quasi-one-dimensional and two-dimensional solutions (systems (9) and (10) respectively; where indistinguishable, dominant style shown): pressure variation in the well (A); respective Reynolds number (B); aperture influx (C); radial pressure profiles in the landfill (D) for outlet and last flowing cross-sections (rightmost, $\ell = 0$, and leftmost, $\ell = L$, curves of identical style respectively). Boundary condition $u(r_{\mathcal{B}}) = 0$. All other parameters listed in appendix A.

cover for a fair span of time. Therefore it is useful to compare flow controllability in these two situations, whose solutions are not a mathematical extension of one another.

4.4 Perforation distribution

Figure 6 depicts the solution for the nominal and double number of perforated sections, with and without halving the number of holes in each. Within the framework of the current analysis losses due to ingress mixing are not modelled. Hence when the total intake area remains constant, the differences are small in the interior well flow (dashed and dotted curves) and stem from changes in the length of uninterrupted pipe flow between apertures due to the non-linearity of (6c). By contrast, simply doubling the number of perforated sections markedly increases the amount of gas collected, in this instance by a factor of about 1.75, but as expected, at the expense of some head losses, more than a twofold total head loss in the well, cf. pressure and Reynolds number. From the solid and dotted curves in the aperture influx panel, figure 6(C), the mass drawn in is notably smaller throughout the well's length, albeit the intake area at each cross-section remains fixed. The respective effect in the landfill is minor, however an interesting phenomenon emerges near the uppermost boundary: a higher value of N is conducive of diminution of the radial velocity, figure 6(E). Thus if the outlet suction required to maintain sub-atmospheric pressure and hence negative radial velocity in the landfill cannot be attained, increasing the number of perforated sections is a viable alternative mechanism to control surface flux.

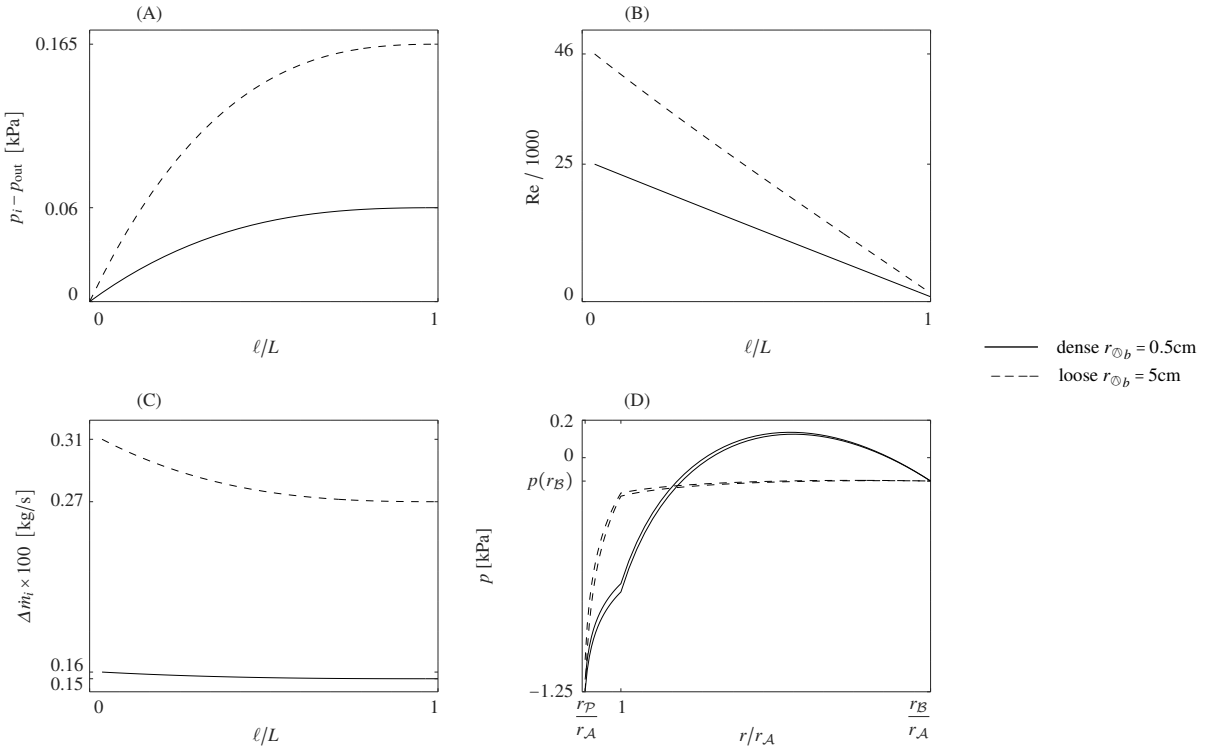

Fig. 4 Solution of system (9) for closely and loosely compacted waste: pressure variation in the well (A); respective Reynolds number (B); aperture influx (C); radial pressure profiles in the landfill (D) for outlet and last flowing cross-sections (rightmost, $\ell = 0$, and leftmost, $\ell = L$, curves of identical style respectively). Outlet pressure $p_{\text{out}} = -1.25$kPa. Boundary condition $p(r_{\mathcal{B}}) = -0.125$kPa. All other parameters listed in appendix A.

5 Surface flux

The solutions in §3, valid within the axisymmetric domain considered, can be extended to estimate flux across the horizontal surface above the landfill. Such an extension requires caution, as the geometry is no longer axisymmetric. Parameter regimes, where the extension applicability deteriorates, are identified hereunder.

The flux through a superficial rectangle $[-\ell_x, \ell_x] \times [0, L]$ (consult figure 1) is given by the integral

$$\dot{m}_s = \int_0^L \int_{-\ell_x}^{\ell_x} \rho u \cos\vartheta \, dx d\ell = 2 \int_0^L \int_{r_{\mathcal{X}}}^{r_x} \rho u \frac{r_{\mathcal{X}} dr d\ell}{\sqrt{r^2 - r_{\mathcal{X}}^2}}, \tag{14a}$$

where $u\cos\vartheta$ is the vertical component of the radial velocity u, the angle ϑ measured from the vertical, $\cos\vartheta = r_{\mathcal{X}}/r$ and $r_x^2 = r_{\mathcal{X}}^2 + \ell_x^2$. Combining with (1), (4a) and (13a), wherein C vanishes, as all gas must be collected from the formal domain Ω (albeit C_b does figure in expressions for various coefficients), yields

$$\dot{m}_s = -\int_0^L \frac{k}{\mu RT} \int_{r_{\mathcal{X}}}^{r_x} \left\{ \frac{a^{(0)}}{r} + \sum_{n=1}^{\infty} \lambda_n \left(a^{(n)} I_1(\tilde{r}) - b^{(n)} K_1(\tilde{r}) \right) \cos\tilde{\ell} \right\} \frac{r_{\mathcal{X}} dr d\ell}{\sqrt{r^2 - r_{\mathcal{X}}^2}}. \tag{14b}$$

For Darcy's law to be conceptually applicable, $\dot{m}_s$ is interpreted as flux immediately beneath the surface. The constants $a^{(0)}$, $a^{(n)}$ and $b^{(n)}$, as well as k, must conform to the respective laminae as the radial integration path crosses the domain. To evaluate the integral one must know what fluid traverses the surface and in which direction. When the pressure at the pipe outlet is not low enough, landfill gas will escape to the atmosphere. When the suction is too strong, air will permeate the

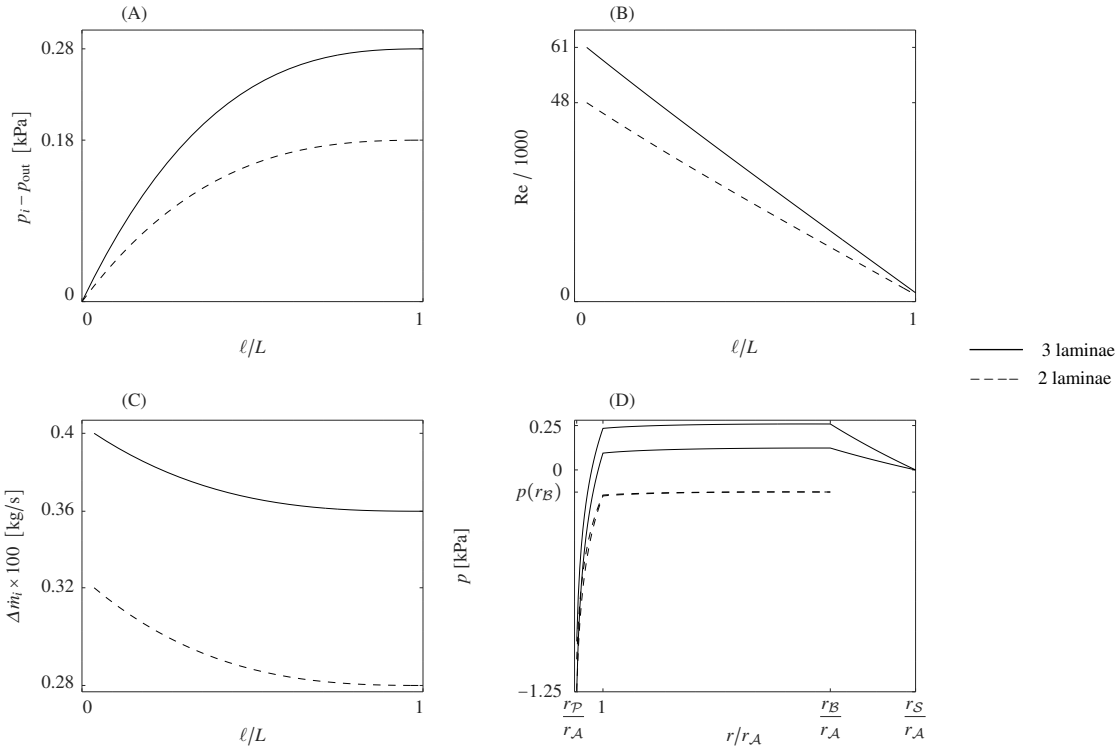

Fig. 5 Solution of system (9) for two and three lamina domains: pressure variation in the well (A); respective Reynolds number (B); aperture influx (C); radial pressure profiles in the landfill (D) for outlet and last flowing cross-sections (rightmost, $\ell = 0$, and leftmost, $\ell = L$, curves of identical style respectively, visually coincident for two laminae). Respective boundary conditions $p(r_{\mathcal{S}}) = p_{\text{bar}}$ and $p(r_{\mathcal{B}}) = -0.125$kPa. Outlet pressure $p_{\text{out}} = -1.25$kPa. All other parameters listed in appendix A.

uppermost lamina. Between these extremities air ingress will be observed close to the outlet, whilst landfill gas will escape further upstream, thereby rendering the fluid properties μ, R and T dependent on the integration variable ℓ, to be determined by the sign of the radial velocity at the top surface: $(+)$ for gas escaping and $(-)$ for air drawn in. If no change of sign occurs, computing the integral $d\ell$ first reveals the sum contributes no flux. Then the remaining integral dr is computed by changing the integration variable to φ via $\cos\varphi = r_{\mathcal{X}}/r$, yielding

$$\dot{m}_s = -\frac{k_x a_x L}{\mu R T} \arctan \frac{\ell_x}{r_{\mathcal{X}}}, \tag{15}$$

where k_x and a_x are the permeability of the outermost lamina in the extended domain and respective logarithmic constant $a^{(0)}$. The parameters μ, R and T must match the fluid actually traversing the surface.

If the radial velocity does change sign, the length ℓ_* such that $u(r, \ell_*) = 0$ must be found, and the integration interval $[0, L]$ divided into $[0, \ell_*]$ and $[\ell_*, L]$, wherein the fluid properties are fixed. No practical simplification ensues in these circumstances, as the integrals

$$\int_1^{r_x/r_{\mathcal{X}}} \frac{I_1(\lambda_n r_{\mathcal{X}} r)}{\sqrt{r^2-1}}\, dr \quad \text{and} \quad \int_1^{r_x/r_{\mathcal{X}}} \frac{K_1(\lambda_n r_{\mathcal{X}} r)}{\sqrt{r^2-1}}\, dr$$

cannot be expressed in terms of standard mathematical functions, and $\dot{m}_s$ was computed numerically by (14b).

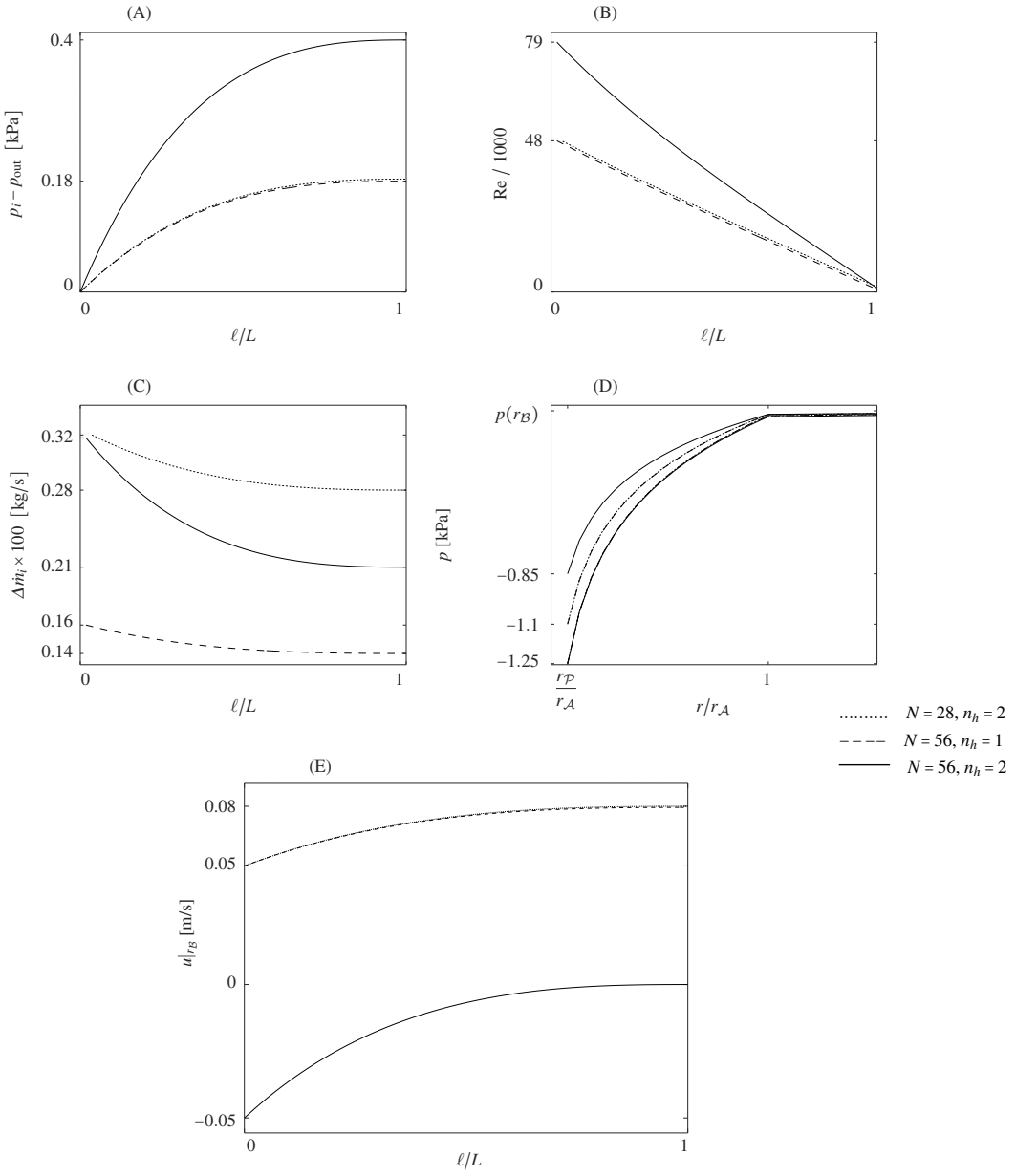

Fig. 6 Solution of system (9) for different perforation configurations: pressure variation in the well (A); respective Reynolds number (B); aperture influx (C); radial pressure profiles in the landfill (D) for outlet and last flowing cross-sections (rightmost, $\ell = 0$, and leftmost, $\ell = L$, curves of identical style respectively, coincident for invariant intake area $Nn_h = 56$); radial velocity at the uppermost landfill surface (E). Outlet pressure $p_{out} = -1.25$kPa. Boundary condition $p(r_B) = -0.125$kPa. All other parameters listed in appendix A.

5.1 Solution extension

In order to extend (13a) for $r > r_X$, C is set to zero, and continuity of both pressure and velocity across the surface $r = r_X$ is imposed, yielding a system of linear equations for coefficients $a_x^{(n)}$ and $b_x^{(n)}$, $n \geqslant 0$. The system doubles in size if the radial path intersects a second discontinuity surface (compare cases $\vartheta \gtrless \vartheta_{cr}$ in figure 1). Closed form expressions, given in appendix D, are instructive from the aspect of qualitative prediction of the parameter regime, where the extension becomes

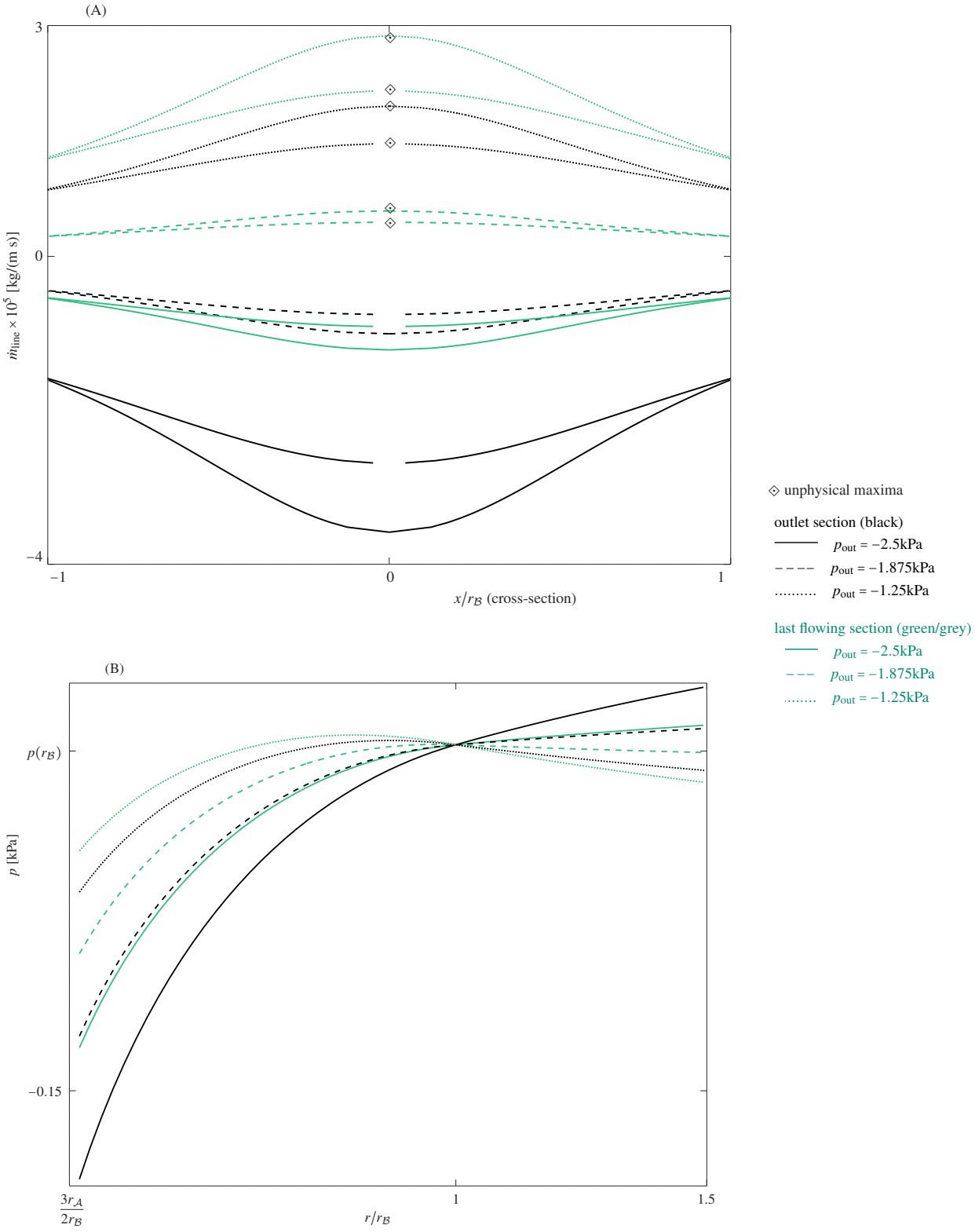

Fig. 7 Impact of outlet suction strength: line flux (A) and respective radial pressure profiles in the landfill (B) for two lamina domain. Boundary condition $p(r_{\mathcal{B}}) = -0.125$kPa. The set of curves with the gap in the centre was obtained when the cover was incorporated for flux computation only (see text). All other parameters listed in appendix A.

inapplicable. One case concerns geometry: $\ell_x/r_{\mathcal{B}} \gg 1$ or $\ell_x/r_{\mathcal{S}} \gg 1$, emphasising that with a solution valid in a finite domain one cannot attain an accurate extrapolation very far from that domain. The second case is related to medium properties: $k_s/k_b \ll 1$, implying that a nearly impervious cover is better modelled as sealed.

Boundary conditions $p(r_{\mathcal{B}}) = p_{\mathcal{B}}$ or $p(r_{\mathcal{S}}) = p_{\mathcal{S}}$ with $\vartheta < \vartheta_{\mathrm{cr}}$ require one seam point. For expositional purposes it is convenient to define line flux, cf. equation (14a), as an integral over the i–th well segment (in the longitudinal direction only):

$$\dot{m}^{(i)}_{\mathrm{line}}(x) = \int_{\ell_{i-1}}^{\ell_i} \rho u \cos\vartheta \, d\ell, \quad 1 \leqslant i \leqslant N. \tag{16}$$

Figure 7 depicts the flux and pressure profiles for the cases of adequate, threshold and insufficient extraction pressure, comparing the outlet and last flowing well segments. The flux was computed to the horizontal distance of 5 times the landfill depth, i.e. $\ell_x = 5r_{\mathcal{B}}$, showing only the central part $x \in (-r_{\mathcal{B}}, r_{\mathcal{B}})$ for clarity. With an adequate outlet suction (solid black and green/grey curves) the flux is negative for all well segments (figure 7(A)), the pressure profiles ascend monotonically for $0 < r < r_{\mathcal{B}}$ (figure 7(B)), and if continued, indicate sub-atmospheric pressure over a fivefold distance away (not shown). Observe that the rate of head loss is always more rapid close to the well outlet, therefore for $r < r_{\mathcal{B}}$ the pressure at the outlet is always lower, whereas for $r > r_{\mathcal{B}}$ the opposite holds. The profiles for all well segments $1 < i < N$ lie between the curves shown in their respective order with no intersections. At some distance $r/r_{\mathcal{B}} > 1$ the pressure profiles will cross the barometric pressure line $p = 0$. These intersections will be monotonically ordered by well segment. The shortest distance will belong to the outlet profile and define the radius of influence for this configuration. The line flux curves are ordered similarly and never intersect. Thus this figure allows to define the well radius of influence r_{I} as the distance, where either radial velocity or line flux exceeds a small negative threshold: $r_{\mathrm{I}} = \min\left\{r \,\middle|\, -u(r;\ell) < u_{\mathrm{th}}\right\}$ or $r_{\mathrm{I}} = \min\left\{x \,\middle|\, -\dot{m}_{\mathrm{line}}(x;\ell) < \dot{m}_{\mathrm{th}}\right\}$, with $u_{\mathrm{th}} > 0$ and $\dot{m}_{\mathrm{th}} > 0$ being the desired thresholds, the minimum taken over all perforated cross-sections.

The dashed curves illustrate a borderline case, where as head is lost upstream from the pipe outlet, the flux becomes positive, i.e. landfill gas flows outwards. The radial pressure profile of the last flowing segment (dashed green/grey curve) manifests a shallow maximum and at the distance $r/r_{\mathcal{B}} \approx 1.5$ is just under the boundary value $p(r_{\mathcal{B}})$. Between the two dashed flux curves there exists a point along the well, past which the radial velocity crosses into the positive region, to wit landfill gas will flow outwards. Thus to obtain a valid radius of influence the definitions above must be supplemented by a caveat the radial velocity remain negative along the well length: whilst r_{I} must be estimated at the outlet, the estimate is valid only if at all upstream sections gas flows inwards (normally the end of the well will give the upper bound).

The dotted curves correspond to a dysfunctional configuration, where proper extraction fails even at the outlet. The pressure profiles have two intersection points with the line $p = p_{\mathcal{B}}$, one conforming to the boundary $r = r_{\mathcal{B}}$ as imposed, the other occurring within the waste lamina. In between the pressure exceeds the prescribed boundary value, attesting to gas accumulation. At the maximum of the pressure profile the radial velocity changes sign and all fluid beyond that point moves outwards, as evidenced by the flux curves.

For all three cases a second set of curves is given, where the cover was incorporated for flux computation only. Mathematically this is possible only for $\vartheta > \vartheta_{\mathrm{cr}}$ (the radial ray to the surface cannot be shorter than the outermost cover radius, limiting the horizontal distance to a positive value), hence the small gaps in the centre. Since these are easily interpolated, their existence is not detrimental in any way. Such an extension supplies an estimate of the mass expected to escape when a landfill cover is frequently removed and replaced. The case of a full solution for three sub-domains with the condition $p(r_{\mathcal{S}}) = p_{\mathcal{S}}$ and $\vartheta \lesseqgtr \vartheta_{\mathrm{cr}}$ lends itself to a qualitatively similar analysis, cf. figure 11 in appendix E.

The extrema of all flux curves are located above the well. With an adequate suction it seems obvious the negative minimum would be located at the smallest possible distance to the well. Counter-intuitively, the location of the positive maximum is identical. Both extrema concur because within the framework of the axisymmetric model the velocity is proportional to the radial pressure gradient (cf. equation (4a)), highest where the suction is strongest. When no suction is applied, the surface flux would be uniform throughout. Therefore it stands to reason that in the proximity of the well even with deficient collection no localised gas escape at a rate in excess of the observed further away should ensue. The shape of the flux curves obtained with the axisymmetric solution is generic, and as shown hereinafter, can be reproduced numerically in other types of domains, as long as an adequate suction is exerted. Past the critical value thereof the shape of the flux curve is unphysical, however the area underneath might be used as an estimate of the total mass escaping.

As head is lost upstream along the well, the minimum becomes shallower, juxtapose, for instance, solid black and green/grey flux curves. Negative flux of landfill gas entails undesirable air ingress into the landfill and is strongest near the outlet. This is not a trivial result due to two conflicting influences. The mass drawn in is proportional to the product

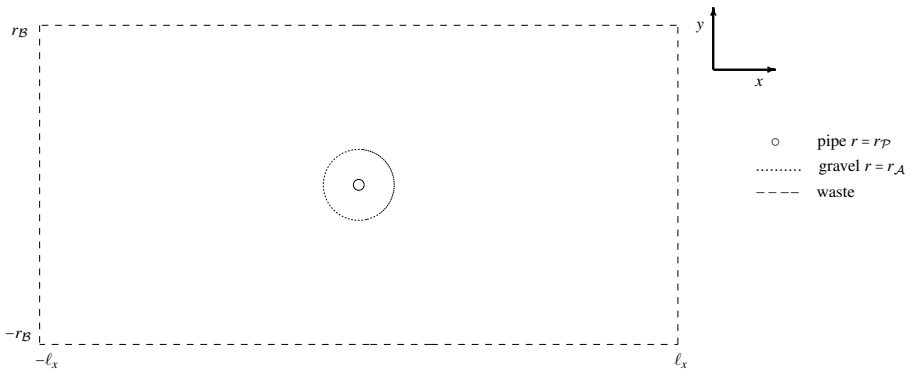

Fig. 8 Flow geometry for finite element solution: pipe and annular gravel lamina imbedded within a rectangular waste layer.

$p|\nabla p|$. Air flow in the porous laminae obeys the same momentum equation (4a), whereby the velocity magnitude diminishes monotonically away from the outlet, whilst the pressure increases. The dominance of the imposed pressure gradient over head loss along the well is confirmed below for domains with no axial symmetry. Therefore only a reduction of suction strength will diminish the influx of air, possibly at the expense of smaller well radius of influence.

5.2 Comparison to finite elements solution

To compare the foregoing results with a setting unencumbered by the assumption of axial symmetry, equation (3) with (4a) was solved in one cross-section on an unstructured triangular, dynamically refined mesh in the finite element solver FlexPDE (PDE Solutions Inc., 2016) with a prescribed relative error in p (non-dimensionalised by $p_{\mathcal{B}}$) of 10^{-5}. Figure 8 shows the domain considered – the pipe and annular gravel lamina imbedded within a rectangular waste layer. The origin is at the centre of the pipe. Define the components of the velocity vector $(\mathfrak{u},\mathfrak{v})^{\mathrm{T}}$ to be the horizontal and vertical fluid velocities. The function $\mathfrak{p}(x,y)$ denotes the pressure. The boundary conditions simulated a landfill with an impermeable membrane lining three sides (standard practice to prevent leachate outflow) and a surface open to the atmosphere:

$$\begin{array}{lll} \mathfrak{u}(x,y)=0 & \text{on} & |x|=\ell_x, \quad |y|\leqslant r_{\mathcal{B}}, \\ \mathfrak{v}(x,y)=0 & \text{on} & y=-r_{\mathcal{B}}, \quad |x|\leqslant \ell_x, \\ \mathfrak{p}(x,y)=p_{\mathcal{B}} & \text{on} & y=r_{\mathcal{B}}, \quad |x|\leqslant \ell_x. \end{array} \tag{17}$$

For compatibility with the axisymmetric solution the generation rate C_b must be scaled by the domain area ratio. Furthermore, the planarity of the finite element solution implies the flux is per unit length in the longitudinal direction, hence requiring a scaling by δ, equation (7). These adjustments render the flux order of magnitude comparable, however no quantitative agreement should be expected.

The first example is a square circumscribing the circle of radius $r_{\mathcal{B}}$

$$\left\{(x,y)\mid -r_{\mathcal{B}}\leqslant x,y\leqslant r_{\mathcal{B}} \text{ and } x^2+y^2\geqslant r_{\mathcal{P}}^2\right\}, \tag{18a}$$

geometrically the closest setting to the axisymmetric one. The pressure on the surface immediately above the well, $\mathfrak{p}(0,r_{\mathcal{B}})$, coincides with the value $p(r_{\mathcal{B}})$ in the axisymmetric solution. The variation of pressure on the vertical sides and flux across the top surface are shown in figure 9 for the three values of suction found to be adequate, borderline and insufficient with the

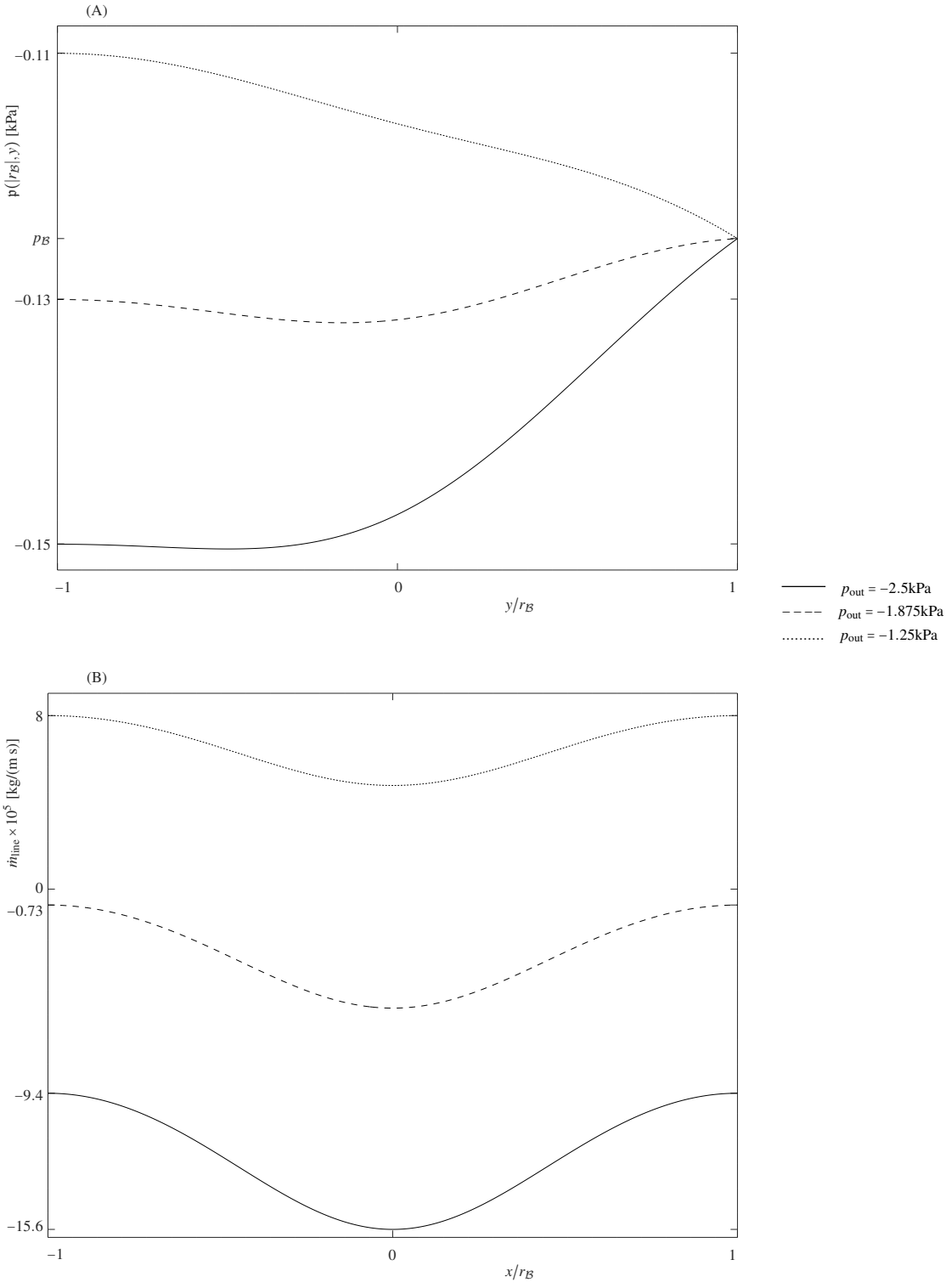

Fig. 9 Impact of outlet suction strength in a square domain (18a): pressure profiles along vertical sides $|x| = r_{\mathcal{B}}$ (A) and line flux (B). Boundary condition on the surface $\mathfrak{p}(x, r_{\mathcal{B}}) = p_{\mathcal{B}} = -0.125$kPa. For compatibility with the axisymmetric solution C_b was scaled by generating lamina area ratio $\left(4r_{\mathcal{B}}^2 - \pi r_{\mathcal{A}}^2\right)\Big/\left(\pi(r_{\mathcal{B}}^2 - r_{\mathcal{A}}^2)\right)$, and flux $\dot{m}_{\text{line}}$ was scaled by δ, equation (7). All other parameters listed in appendix A.

axisymmetric model (figure 7). The flux curves' sign confirms those findings, albeit the pressure profiles are quite dissimilar (cf. figure 7) due to the no flux condition. The minima become shallower with diminution of the suction strength, but at no time morph into maxima.

The second example is a rectangular domain of the width taken for the extension of the axisymmetric solution

$$\Big\{(x,y) \mid -5r_{\mathcal{B}} \leqslant x \leqslant 5r_{\mathcal{B}},\ -r_{\mathcal{B}} \leqslant y \leqslant r_{\mathcal{B}} \ \text{ and } \ x^2+y^2 \geqslant r_{\mathcal{P}}^2\Big\}, \tag{18b}$$

and boundary conditions as in (17). Figure 10 depicts the pressure profiles at the same horizontal distance $|x| = r_{\mathcal{B}}$. Because the no flux boundaries $|x| = 5r_{\mathcal{B}}$ are fairly far away, the profiles are redolent of the axisymmetric ones (figure 7). The flux curves' sign indicates air infiltration near the well and landfill gas escape at a certain distance for all three suction values. The root location bears on the quality of prediction to be anticipated from the axisymmetric model: the dotted and solid curves, corresponding to the weakest and strongest suction values, just become positive at $|x| \approx r_{\mathcal{B}}$ and $|x| \approx 2r_{\mathcal{B}}$ respectively, i.e. in this case the extension of the axisymmetric solution likely grows unreliable for $\ell_x \gtrapprox 2r_{\mathcal{X}}$. Observe that the escape rate predicted with the axisymmetric model should be regarded as a low bound for two reasons. One, in a domain with no axial symmetry the fluid need not traverse an additional expanse of hydrodynamically resistant medium. Two, with the underground sides impermeable any fluid leaving the domain must do so through the surface, whilst in an axisymmetric domain the fluid leaves through the entire circumference, some never reaching the surface.

In summary, albeit no realistic landfill flow is faithfully described by an axisymmetric flow field, the model reproduces basic features of qualitative import: pressure profiles in the porous media under comparable conditions and surface flux for adequate suction values.

6 Discussion

Collection of landfill gas by a horizontal well was analysed as an axisymmetric flow through a porous medium coupled to a weakly compressible pipe flow within the well. The study successfully reconstructed realistic extraction, offered an analytical explanation to three control associated phenomena observed in the field and identified parameter combinations conducive of their occurrence.

(A) At times the operator is able to control the well flow rate through the outlet suction, whilst at others it proved impossible. The analysis showed that these situations could be expected for partly permeable and sealed cover layers respectively. More generally, a cover permeability many orders of magnitude smaller than that of the waste lamina will result in a difficulty to use the outlet sub-atmospheric pressure as a control mechanism. Then the aperture spacing becomes the main means of control available. It is conjectured that the number and azimuthal distribution of apertures within the same perforated cross-section will not provide effective flow control, since the main head losses occur in the porous medium. Albeit losses due to entry into the well and mixing exist, they are expected to be secondary by comparison.

(B) For certain types of refuse a high production is expected owing to the abundance of carbon, e.g. when a significant fraction of the waste is household garbage or organic matter. However at times this expectation was not vindicated in the field despite a seemingly adequate suction strength. The source of this difficulty lies in a low waste to gravel permeability ratio due to the ease of initial compacting. The generation rate is indeed high and the gas accumulates in the landfill. The effective resistance of the landfill must be reduced for proper collection, an end most effectively attained through an increase in perforation density.

(C) Air infiltration is detrimental to the population of bacteria responsible for waste degradation. The mass drawn in is proportional to $p|\nabla p|$, with the pressure and its radial gradient growing monotonically toward opposite ends of the well. The gradient was shown to be dominant, implying maximal infiltration at the outlet and diminution of suction strength as its control mechanism. Aperture spacing or area can be used to compensate for lesser landfill gas collection.

For a fixed outlet suction strength the radius of influence of a well is defined as the largest horizontal distance, where landfill gas will be collected. The current solution framework allows to obtain the radius of influence as the maximal well depth such that no gas escapes to the atmosphere; obtain the horizontal distance where the efflux of landfill gas and/or influx of air are within prescribed regulation limits; estimate the required permeability of a cover to prevent interchange of gas with the atmosphere.

The purpose herein was to model the system with basic flow equations, employing relatively few parameters that a design engineer can readily estimate. High precision in the values thereof is not imperative and in fact would be meaningless. When a parameter value is not accessible with certainty, the correct approach would be to obtain solutions for a range of values and examine the sensitivity ensuing.

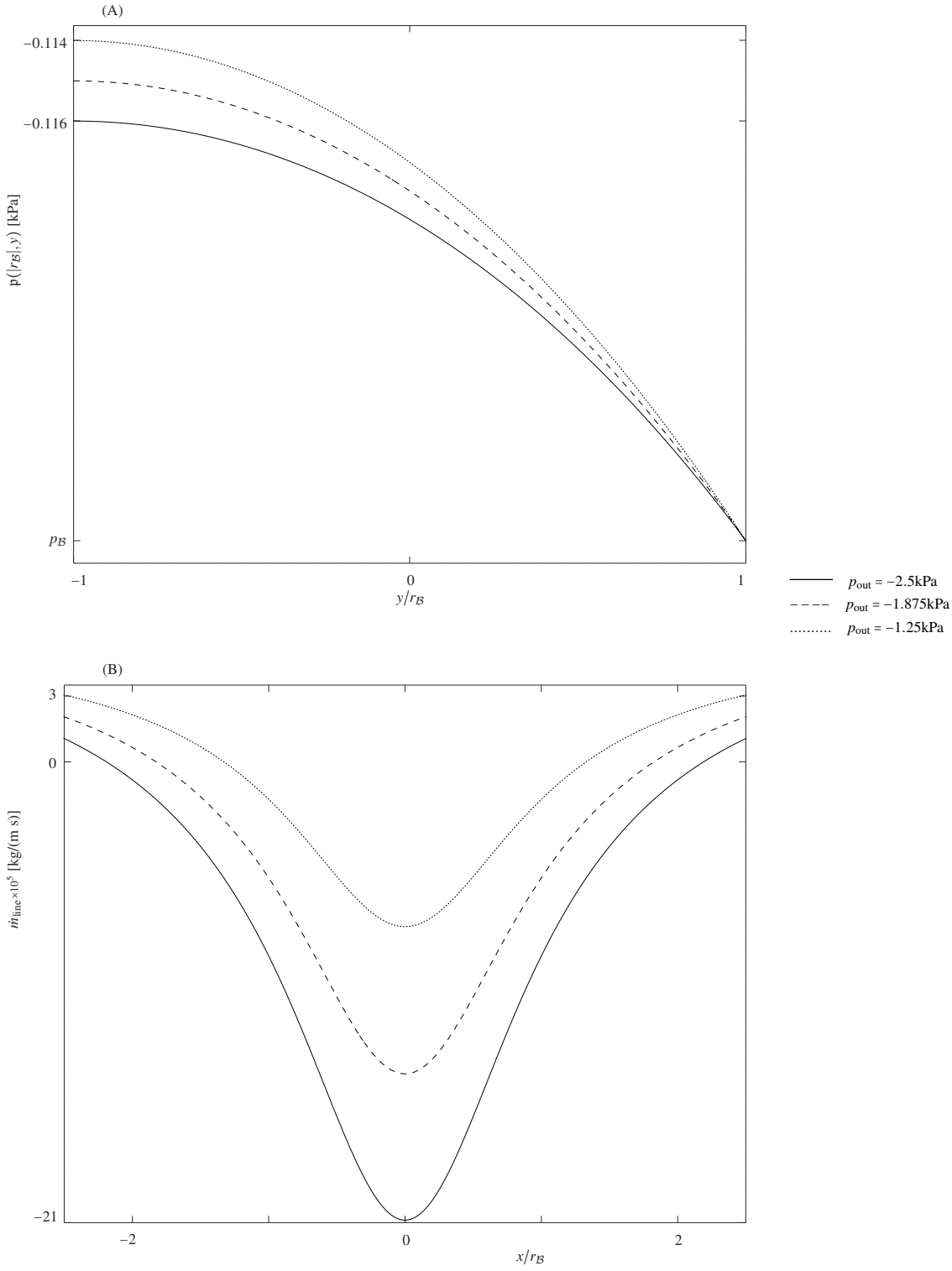

Fig. 10 Impact of outlet suction strength in a rectangular domain (18b): pressure profiles along vertical sides $|x| = r_{\mathcal{B}}$ (A) and line flux (B). Boundary condition on the surface $\mathfrak{p}(x, r_{\mathcal{B}}) = p_{\mathcal{B}} = -0.125$kPa. For compatibility with the axisymmetric solution C_b was scaled by generating lamina area ratio $\left(20r_{\mathcal{B}}^2 - \pi r_{\mathcal{A}}^2\right)\Big/\left(\pi(r_{\mathcal{B}}^2 - r_{\mathcal{A}}^2)\right)$, and flux $\dot{m}_{\text{line}}$ was scaled by δ, equation (7). All other parameters listed in appendix A.

In summary, effective resistance to fluid flow in this system stems from two unrelated sources: permeability ratios between the various medium layers and spacing between perforated cross-sections. A no flux boundary condition is equivalent to an additional layer of zero permeability and thus infinite ratios for all other layers. In practice layers of very low permeability will give rise to phenomena observed with no flux conditions. Educated manipulation of permeability ratios and aperture density are two reliable control mechanisms, whereas the more intuitive suction strength at times fails to attain the desired efficacy of collection. In the control of air infiltration a non-uniform perforation density is a feature of interest to be explored.

The head losses within the landfill were found to be quite small, especially if the waste to gravel layer permeability ratio is on the characteristic scale of 10. Therefore gravity might be a non-negligible factor in the vertical balance of momentum. Since breaking the axial symmetry renders the flow equations analytically intractable, a numerical solution of a gravity inclusive system is a topic of future research.

Acknowledgement

Field data furnished by GNH Consulting Ltd., Delta, British Columbia, Canada, are gratefully acknowledged.

References

Allan FM, Hajii MA, Anwar MN (2008) The characteristics of fluid flow through multilayer porous media. J Appl Mech 76(1):014501

Bahloul A, Yahiaoui MA, Vasseur P, Bennacer R, Beji H (2005) Natural convection of a two-component fluid in porous media bounded by tall concentric vertical cylinders. J Appl Mech 73(1):26–33

Carman PC (1937) Fluid flow through granular beds. Transactions of Institution of Chemical Engineers 15:150–167

Chen YC, Chen KS, Wu CH (2003) Numerical simulation of gas flow around a passive vent in a sanitary landfill. Journal of Hazardous Materials B 100:39–52

Colebrook CF (1939) Turbulent flow in pipes, with particular reference to the transition region between the smooth and rough pipe laws. Journal of the Institution of Civil Engineers 11:133–156

Davidson TA (1993) A simple and accurate method for calculating viscosity of gaseous mixtures. Report of investigations, US Department of the Interior, Bureau of Mines.

Fand RM, Kim BYK, Lam ACC, Phan RT (1987) Resistance to the flow of fluids through simple and complex porous media whose matrices are composed of randomly packed spheres. J Fluids Eng 109:268–273

Feng SJ, Zheng QT, Xie HJ (2015) A model for gas pressure in layered landfills with horizontal gas collection systems. Comput Geotech 68:117–127

Feng SJ, Zheng QT, Xie HJ (2017) A gas flow model for layered landfills with vertical extraction wells. Waste Management 66:101–113

Fulks WB, Guenther RB, Roetman EL (1971) Equations of motion and continuity for fluid flow in a porous medium. Acta Mechanica 12:121–129

Gradshteyn IS, Ryzhik IM (2007) Table of integrals, series and products. 7th edition, edited by Alan Jeffrey and Daniel Zwillinger, Academic Press, Elsevier; identities 8.405-8.407, 8.472, 8.477

Henderson N, Brêttas JC, Sacco WF (2010) A three-parameter Kozeny-Carman generalized equation for fractal porous media. Chemical Engineering Science 65:4432–4442

Lage JL, Anthohe BV, Nield DA (1997) Two types of nonlinear pressure-drop versus flow-rate relation observed for saturated porous media. J Fluids Eng 119:700–706

Nakshatrala KB, Joodat SHS, Ballarini R (2018) Modeling flow in porous media with double porosity/permeability: mathematical model, properties and analytical solutions. J Appl Mech 85(8):081009

Nec Y, Huculak G (2017) Solution of weakly compressible isothermal flow in landfill gas collection networks. Fluid Dynamics Research 49:065505

Panda MN, Lake LW (1994) Estimation of single-phase permeability from parameters of particle-size distribution. American Association of Petroleum Geologists Bulletin 78(7):1028–1039

PDE Solutions Inc. (2016) Flexpde 7. *http://www.pdesolutions.com*

Whitaker S (1986) Flow in porous media I: a theoretical derivation of Darcy's law. Transport in Porous Media 1:3–25

Yu L, Batlle F, Carrera J, Lloret A (2009) Gas flow to a vertical gas extraction well in deformable MSW landfills. Journal of Hazardous Materials 168:1404–1416

Appendix A. Nominal parameters

Table 1 lists the nominal set of parameters used in computations throughout unless noted specifically in pertinent figure captions. All geometric quantities are from an existing demolition, land clearing and construction (DLC) landfill. Gas composition and temperature are typical directly measured values. Pipe roughness ε is in accord with the installed pipe material. Equivalent particle radius $r_{\textcircled{s}}$ and porosity were derived from estimated waste fragment size. Gas generation rate C_b was inferred from production values and landfill dimensions. The rightmost column in table 1 gives the ranges for which the iterative schemes' performance and in particular the convergence of series (13a) satisfied the uniform criteria set respectively in §4 and §3.2.

parameter	symbol	value	test range
pipe radius	$r_{\mathcal{P}}$	0.0762m	$(3r_{\mathcal{P}}/4, 2r_{\mathcal{P}})$
tortuosity	τ	125	$(\tau/5, 10\tau)$
temperature	T	15^oC	$(0, 1000)^o$C
pipe roughness	ε	1.5×10^{-6}m	$(\varepsilon/100, 1000\varepsilon)$
hole radius	r_h	0.00476m	$(r_h/2, 2r_h)$
generation rate	C_b	0.004kg/(m^{3}hr)	$(0, 20C_b)$
CH_4 molar fraction	x_{CH_4}	0.5	(0,1)
O_2 molar fraction	x_{O_2}	0.01	(0,1)
CO_2 molar fraction	x_{CO_2}	0.4	(0,1)
# of perforated sections	N	28	$(N/2, 2N)$
total well length	L	420m	$(L/15, 2L)$
# of holes per section	n_h	2	(1,5)

parameter	gravel lamina $\mathcal{PA}$	waste lamina $\mathcal{AB}$	cover lamina $\mathcal{BS}$	test range
thickness h	1m	8m	3m	$(h/2, 3h/2)$
porosity ϕ	0.4	0.6	0.5	(0.2,0.9)
particle radius $r_{\textcircled{s}}$	0.025m	0.05m	0.005m	$(r_{\textcircled{s}}/10, 5r_{\textcircled{s}})$

Table 1 Parameters common to all examples solved numerically, courtesy of GNH Consulting Ltd. The rightmost column gives the ranges for which sound numerical solutions were obtained (consult §4 and §3.2 for criteria).

Appendix B. Coefficients for radial flow

For any section $i \in \{0,\dots,N\}$ (index 0 conforms to the outlet plane and $1 \leqslant i \leqslant N$ to perforated sections)

$$\text{case } p(r_{\mathcal{B}}) = p_{\mathcal{B}}: \qquad p^2 = \begin{cases} p_i^2 + a_a^{(0)} \ln\dfrac{r}{r_{\mathcal{P}}} & r_{\mathcal{P}} \leqslant r \leqslant r_{\mathcal{A}} \\ p_{\mathcal{B}}^2 + \dfrac{\mu}{2k_b} RTC_b\left(r_{\mathcal{B}}^2 - r^2\right) + a_b^{(0)} \ln\dfrac{r}{r_{\mathcal{B}}} & r_{\mathcal{A}} \leqslant r \leqslant r_{\mathcal{B}}, \end{cases} \tag{B1}$$

$$a_a^{(0)} = \left\{ p_{\mathcal{B}}^2 - p_i^2 + \frac{\mu}{k_b} RTC_b \left(\frac{1}{2}\left(r_{\mathcal{B}}^2 - r_{\mathcal{A}}^2\right) + r_{\mathcal{A}}^2 \ln\frac{r_{\mathcal{A}}}{r_{\mathcal{B}}} \right) \right\} \Bigg/ \left\{ \ln\frac{r_{\mathcal{A}}}{r_{\mathcal{P}}} - \frac{k_a}{k_b} \ln\frac{r_{\mathcal{A}}}{r_{\mathcal{B}}} \right\},$$

$$a_b^{(0)} = \frac{k_a}{k_b}\, a_a^{(0)} + \frac{\mu}{k_b} RTC_b r_{\mathcal{A}}^2,$$

$$\text{case } p(r_{\mathcal{S}}) = p_{\mathcal{S}}: \qquad p^2 = \begin{cases} p_i^2 + a_a^{(0)} \ln\dfrac{r}{r_{\mathcal{P}}} & r_{\mathcal{P}} \leqslant r \leqslant r_{\mathcal{A}} \\ p_{\mathcal{S}}^2 + a_s^{(0)} \ln\dfrac{r_{\mathcal{B}}}{r_{\mathcal{S}}} + \dfrac{\mu}{2k_b} RTC_b\left(r_{\mathcal{B}}^2 - r^2\right) + a_b^{(0)} \ln\dfrac{r}{r_{\mathcal{B}}} & r_{\mathcal{A}} \leqslant r \leqslant r_{\mathcal{B}} \\ p_{\mathcal{S}}^2 + a_s^{(0)} \ln\dfrac{r}{r_{\mathcal{S}}} & r_{\mathcal{B}} \leqslant r \leqslant r_{\mathcal{S}} \end{cases} \tag{B2}$$

$$a_a^{(0)} = \left\{ p_{\mathcal{S}}^2 - p_i^2 + \frac{\mu}{k_b} RTC_b \left(\frac{1}{2}\left(r_{\mathcal{B}}^2 - r_{\mathcal{A}}^2\right) + r_{\mathcal{A}}^2 \ln \frac{r_{\mathcal{A}}}{r_{\mathcal{B}}} \right) - \frac{\mu}{k_s} RTC_b \left(r_{\mathcal{B}}^2 - r_{\mathcal{A}}^2\right) \ln \frac{r_{\mathcal{B}}}{r_{\mathcal{S}}} \right\} \Bigg/ \left\{ \ln \frac{r_{\mathcal{A}}}{r_{\mathcal{P}}} - \frac{k_a}{k_b} \ln \frac{r_{\mathcal{A}}}{r_{\mathcal{B}}} - \frac{k_a}{k_s} \ln \frac{r_{\mathcal{B}}}{r_{\mathcal{S}}} \right\},$$

$$a_b^{(0)} = \frac{k_a}{k_b}\, a_a^{(0)} + \frac{\mu}{k_b} RTC_b\, r_{\mathcal{A}}^2,$$

$$a_s^{(0)} = \frac{k_a}{k_s}\, a_a^{(0)} + \frac{\mu}{k_s} RTC_b \left(r_{\mathcal{A}}^2 - r_{\mathcal{B}}^2\right),$$

$$\text{cases } u(r_{\mathcal{X}}) = 0: \qquad p^2 = \begin{cases} p_i^2 + \dfrac{\mu}{k_a} RTC_b \left(r_{\mathcal{B}}^2 - r_{\mathcal{A}}^2\right) \ln \dfrac{r}{r_{\mathcal{P}}} & r_{\mathcal{P}} \leqslant r \leqslant r_{\mathcal{A}} \\ p_i^2 + \mu RTC_b \left\{ \dfrac{r_{\mathcal{A}}^2 - r^2}{2k_b} + \dfrac{r_{\mathcal{B}}^2}{k_b} \ln \dfrac{r}{r_{\mathcal{A}}} + \dfrac{r_{\mathcal{B}}^2 - r_{\mathcal{A}}^2}{k_a} \ln \dfrac{r_{\mathcal{A}}}{r_{\mathcal{P}}} \right\} & r_{\mathcal{A}} \leqslant r \leqslant r_{\mathcal{B}} \\ p_i^2 + \mu RTC_b \left\{ \left(r_{\mathcal{A}}^2 - r_{\mathcal{B}}^2\right) \left(\dfrac{1}{2k_b} - \dfrac{1}{k_a} \ln \dfrac{r_{\mathcal{A}}}{r_{\mathcal{P}}} \right) + \dfrac{r_{\mathcal{B}}^2}{k_b} \ln \dfrac{r_{\mathcal{B}}}{r_{\mathcal{A}}} \right\} & r_{\mathcal{B}} \leqslant r \leqslant r_{\mathcal{S}}. \end{cases} \tag{B3}$$

In all foregoing equations subscripts $(\cdot)_a$, $(\cdot)_b$ and $(\cdot)_s$ correspond to laminae $\mathcal{PA}$, $\mathcal{AB}$ and $\mathcal{BS}$ respectively (consult figure 1). Cases $u(r_{\mathcal{B}}) = 0$ and $u(r_{\mathcal{S}}) = 0$ were unified in (B3), as by (11) within $\mathcal{BS}$, a lamina with no gas generation, a condition of zero velocity at $u(r_{\mathcal{S}}) = 0$ implies constant pressure and no flow, so that in fact $u = 0 \;\forall\; r_{\mathcal{B}} \leqslant r \leqslant r_{\mathcal{S}}$.

Appendix C. Coefficients for radial-longitudinal flow

For any $n \geqslant 1$ the coefficients in (13a) are given below. The stretched coordinates $(\tilde{r}, \tilde{\ell})$ defined in (13b) are used with subscripts identical to the plain coordinates (r, ℓ). For two laminae

$$a_b^{(n)} = \frac{2K_0(\tilde{r}_{\mathcal{B}})}{\tilde{r}_{\mathcal{A}} L} \int_0^L p_{\text{in}}^2(\ell) \cos \tilde{\ell} d\ell \Bigg/ \left\{ M_{00}^-(\tilde{r}_{\mathcal{A}}, \tilde{r}_{\mathcal{B}}) M_{01}^+(\tilde{r}_{\mathcal{P}}, \tilde{r}_{\mathcal{A}}) + M_{10}^+(\tilde{r}_{\mathcal{A}}, \tilde{r}_{\mathcal{B}}) M_{00}^-(\tilde{r}_{\mathcal{P}}, \tilde{r}_{\mathcal{A}}) \frac{k_b}{k_a} \right\}, \tag{C1}$$

$$b_b^{(n)} = -a_b^{(n)}\, I_0(\tilde{r}_{\mathcal{B}}) \Big/ K_0(\tilde{r}_{\mathcal{B}}),$$

$$\begin{pmatrix} a_a^{(n)} \\ b_a^{(n)} \end{pmatrix} = \frac{a_b^{(n)} \tilde{r}_{\mathcal{A}}}{K_0(\tilde{r}_{\mathcal{B}})} \begin{pmatrix} K_1(\tilde{r}_{\mathcal{A}}) & K_0(\tilde{r}_{\mathcal{A}}) k_b/k_a \\ I_1(\tilde{r}_{\mathcal{A}}) & -I_0(\tilde{r}_{\mathcal{A}}) k_b/k_a \end{pmatrix} \begin{pmatrix} M_{00}^-(\tilde{r}_{\mathcal{A}}, \tilde{r}_{\mathcal{B}}) \\ M_{10}^+(\tilde{r}_{\mathcal{A}}, \tilde{r}_{\mathcal{B}}) \end{pmatrix},$$

$$M_{ij}^{\pm}(\zeta_1, \zeta_2) = I_i(\zeta_1) K_j(\zeta_2) \pm I_j(\zeta_2) K_i(\zeta_1), \quad i, j \in \mathbb{Z}^{\geqslant}.$$

With three laminae the solution is given in matrix form, as there is little to be gained by writing out the explicit quite cumbersome formulae:

$$\begin{pmatrix} a_a^{(n)} & b_a^{(n)} & a_b^{(n)} & b_b^{(n)} & a_s^{(n)} & b_s^{(n)} \end{pmatrix}^{\mathrm{T}} = \mathcal{M}^{-1} \begin{pmatrix} \dfrac{2}{L} \displaystyle\int_0^L p_{\text{in}}^2(\ell) \cos \tilde{\ell} d\ell & 0 & 0 & 0 & 0 & 0 \end{pmatrix}^{\mathrm{T}}, \tag{C2}$$

$$\mathcal{M} = \begin{pmatrix} \mathcal{M}_1 & Z \\ Z & \mathcal{M}_2 \end{pmatrix},$$

$$\mathcal{M}_1 = \begin{pmatrix} I_0(\tilde{r}_{\mathcal{P}}) & K_0(\tilde{r}_{\mathcal{P}}) & 0 & 0 \\ I_0(\tilde{r}_{\mathcal{A}}) & K_0(\tilde{r}_{\mathcal{A}}) & -I_0(\tilde{r}_{\mathcal{A}}) & -K_0(\tilde{r}_{\mathcal{A}}) \\ I_1(\tilde{r}_{\mathcal{A}}) \dfrac{k_a}{k_b} & -K_1(\tilde{r}_{\mathcal{A}}) \dfrac{k_a}{k_b} & -I_1(\tilde{r}_{\mathcal{A}}) & K_1(\tilde{r}_{\mathcal{A}}) \end{pmatrix}$$

$$\mathcal{M}_2 = \begin{pmatrix} 0 & 0 & I_0(\tilde{r}_{\mathcal{S}}) & K_0(\tilde{r}_{\mathcal{S}}) \\ -I_0(\tilde{r}_{\mathcal{B}}) & -K_0(\tilde{r}_{\mathcal{B}}) & I_0(\tilde{r}_{\mathcal{B}}) & K_0(\tilde{r}_{\mathcal{B}}) \\ -I_1(\tilde{r}_{\mathcal{B}}) & K_1(\tilde{r}_{\mathcal{B}}) & I_1(\tilde{r}_{\mathcal{B}}) \dfrac{k_s}{k_b} & -K_1(\tilde{r}_{\mathcal{B}}) \dfrac{k_s}{k_b} \end{pmatrix},$$

and Z is a 3×2 zero matrix. For the case of vanishing velocity

$$a_b^{(n)} = \frac{2K_1(\tilde{r}_{\mathcal{B}})}{\tilde{r}_{\mathcal{A}} L} \int_0^L p_{\text{in}}^2(\ell) \cos \tilde{\ell} d\ell \Bigg/ \left\{ M_{01}^+(\tilde{r}_{\mathcal{A}}, \tilde{r}_{\mathcal{B}}) M_{01}^+(\tilde{r}_{\mathcal{P}}, \tilde{r}_{\mathcal{A}}) + M_{11}^-(\tilde{r}_{\mathcal{A}}, \tilde{r}_{\mathcal{B}}) M_{00}^-(\tilde{r}_{\mathcal{P}}, \tilde{r}_{\mathcal{A}}) \frac{k_b}{k_a} \right\}, \tag{C3}$$

$$b_b^{(n)} = a_b^{(n)}\, I_1(\tilde r_{\mathcal B})\Big/K_1(\tilde r_{\mathcal B}),$$

$$\begin{pmatrix} a_a^{(n)} \\ b_a^{(n)} \end{pmatrix} = \frac{a_b^{(n)}\tilde r_{\mathcal A}}{K_1(\tilde r_{\mathcal B})} \begin{pmatrix} K_1(\tilde r_{\mathcal A}) & K_0(\tilde r_{\mathcal A})k_b/k_a \\ I_1(\tilde r_{\mathcal A}) & -I_0(\tilde r_{\mathcal A})k_b/k_a \end{pmatrix} \begin{pmatrix} M_{01}^{+}(\tilde r_{\mathcal A}, \tilde r_{\mathcal B}) \\ M_{11}^{-}(\tilde r_{\mathcal A}, \tilde r_{\mathcal B}) \end{pmatrix},$$

$$a_s^{(n)} = b_s^{(n)} = 0,$$

the vanishing coefficients applicable if $r_{\mathcal X} = r_{\mathcal S}$.

Appendix D. Coefficients for solution extension

Denoting the external domain with the subscript $(\,\cdot\,)_x$ and demanding continuity of both pressure and velocity across the radius $r = r_{\mathcal X}$

$$p(r_{\mathcal X}^{-}, \ell) = p(r_{\mathcal X}^{+}, \ell), \quad \left(k\frac{\partial p}{\partial r}\right)_{(r_{\mathcal X}^{-}, \ell)} = \left(k\frac{\partial p}{\partial r}\right)_{(r_{\mathcal X}^{+}, \ell)} \tag{D1}$$

yields a system of linear equations, whose solution is

$$a_{\mathcal X}^{(0)} = \frac{k(r_{\mathcal X}^{-})}{k(r_{\mathcal X}^{+})}\, a^{(0)} - \frac{\mu}{k(r_{\mathcal X}^{+})} RTC r_{\mathcal X}^2, \tag{D2}$$

$$b_{\mathcal X}^{(0)} = \left(a^{(0)} - a_{\mathcal X}^{(0)}\right)\ln r_{\mathcal X} + b^{(0)} - \frac{\mu}{2k(r_{\mathcal X}^{-})} RTC r_{\mathcal X}^2,$$

and for $n \geqslant 1$

$$\begin{pmatrix} a_{\mathcal X}^{(n)} \\ b_{\mathcal X}^{(n)} \end{pmatrix} = \mathcal M_{\mathcal X}^{-1} \begin{pmatrix} I_0(\tilde r_{\mathcal X}) & K_0(\tilde r_{\mathcal X}) \\ \dfrac{k(r_{\mathcal X}^{-})}{k(r_{\mathcal X}^{+})} I_1(\tilde r_{\mathcal X}) & -\dfrac{k(r_{\mathcal X}^{-})}{k(r_{\mathcal X}^{+})} K_1(\tilde r_{\mathcal X}) \end{pmatrix} \begin{pmatrix} a^{(n)} \\ b^{(n)} \end{pmatrix}, \qquad \mathcal M_{\mathcal X} = \begin{pmatrix} I_0(\tilde r_{\mathcal X}) & K_0(\tilde r_{\mathcal X}) \\ I_1(\tilde r_{\mathcal X}) & -K_1(\tilde r_{\mathcal X}) \end{pmatrix}. \tag{D3}$$

Since $\det \mathcal M_{\mathcal X} = -1/\tilde r_{\mathcal X} \neq 0$, solution (D3) always exists. If $k(r_{\mathcal X}^{-}) = k(r_{\mathcal X}^{+})$ and with the generation rate in the outermost lamina of the solution domain vanishing, i.e. $C = 0$, the extension coefficients satisfy $a_{\mathcal X}^{(n)} = a^{(n)}$, $b_{\mathcal X}^{(n)} = b^{(n)}$ for any $n \geqslant 0$. The closed form extension coefficients in two dimensions ensue by (D1) and are cumbersome, whilst not being particularly instructive. Therefore they are omitted here, notwithstanding being fully implemented in the computations for all presented examples. Expressions for the quasi-one-dimensional solution, being the leading order terms, are given for all considered boundary conditions.

Denoting the external domain with the subscript $(\,\cdot\,)_x$. for the boundary condition $p(r_{\mathcal B}) = p_{\mathcal B}$

$$p^2 = p_{\mathcal B}^2 + a_x \ln\frac{r}{r_{\mathcal B}}, \quad a_x = -2\mu u(r_{\mathcal B}) p_{\mathcal B} r_{\mathcal B}\big/k_b \qquad r_{\mathcal B} \leqslant r \leqslant r_x\big|_{\mathcal B}, \tag{D4}$$

$r_{\mathcal B}$ being the sole seam point. With a permeable cover included post-solution two seam points are required. One, when crossing the formal domain at $r_{\mathcal B}$: the generation rate becomes $C = 0$. Two, when moving along a radial ray, one arrives at the horizontal line $\mathcal B$ in figure 1, where the permeability changes. Then

$$p^2 = \begin{cases} p_{\mathcal B}^2 + a_x \ln\dfrac{r}{r_{\mathcal B}} & r_{\mathcal B} \leqslant r \leqslant r_x\big|_{\mathcal B} \\ p^2\left(r_x\big|_{\mathcal B}\right) + a_x \dfrac{k_b}{k_s} \ln\dfrac{r}{r_x\big|_{\mathcal B}} & r_x\big|_{\mathcal B} \leqslant r \leqslant r_x\big|_{\mathcal S}. \end{cases} \tag{D5}$$

The radii $r_x\big|_{\mathcal B}$ and $r_x\big|_{\mathcal S}$ are the points, where a radial ray intersects the horizontal lines $\mathcal B$ and $\mathcal S$ and thus vary with ℓ_x.

The case $p(r_{\mathcal S}) = p_{\mathcal S}$ is conceptually disparate from the extension case (D5) in that the boundary pressure $p_{\mathcal S}$ is not inferred, but dictated. Here two possibilities arise. One, ℓ_x is relatively small, so that the angle created by drawing a radial ray from the pipe centre to the end of the segment ℓ_x falls within ϑ_{cr} in figure 1. Within that sector one seam point is required. Outside of ϑ_{cr} two seam points are necessary:

$$\vartheta < \vartheta_{\mathrm{cr}} \qquad p^2 = p_{\mathcal S}^2 + a_x \ln\frac{r}{r_{\mathcal S}}, \quad a_x = -2\mu u(r_{\mathcal S}) p_{\mathcal S} r_{\mathcal S}\big/k_s \qquad r_{\mathcal S} \leqslant r \leqslant r_x\big|_{\mathcal S}, \tag{D6}$$

$$\vartheta \geqslant \vartheta_{\mathrm{cr}} \qquad p^2 = \begin{cases} p_{\mathcal S}^2 + a_x \dfrac{k_s}{k_b} \ln\dfrac{r}{r_{\mathcal S}} & r_{\mathcal S} \leqslant r \leqslant r_x\big|_{\mathcal B} \\ p^2\left(r_x\big|_{\mathcal B}\right) + a_x \ln\dfrac{r}{r_x\big|_{\mathcal B}} & r_x\big|_{\mathcal B} \leqslant r \leqslant r_x\big|_{\mathcal S}. \end{cases} \tag{D7}$$

If the radial velocity at $r_{\mathcal B}$ vanishes, the surface flux is zero since $p = p(r_{\mathcal B})$ when $r \geqslant r_{\mathcal B}$.

Appendix E. Surface flux: three sub-domains

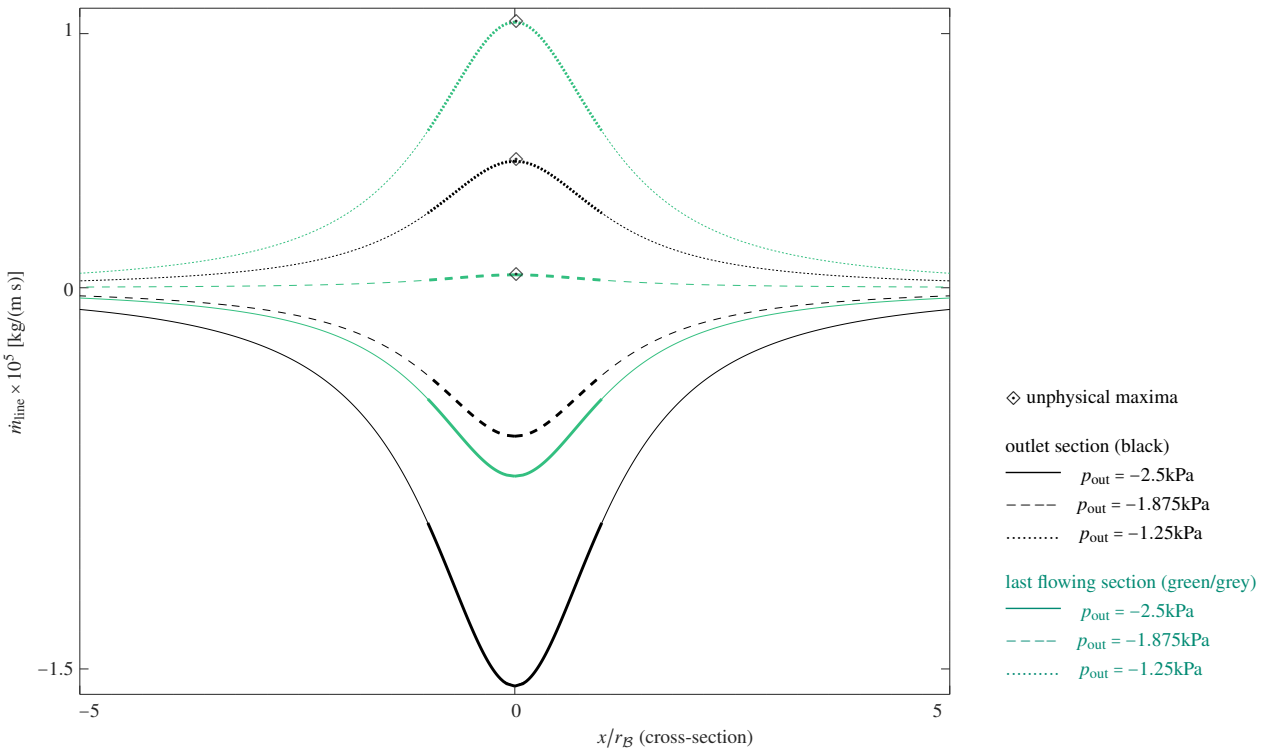

Fig. 11 Impact of outlet suction strength: line flux for three lamina domain. Centred thick curves correspond to $|\vartheta| < \vartheta_{\mathrm{cr}}$. Boundary condition $p(r_{\mathcal{S}}) = p_{\mathrm{bar}}$. All other parameters listed in appendix A.